HHS Public Access

Author manuscript

Nat Cancer. Author manuscript; available in PMC 2021 December 01.

Published in final edited form as:

Nat Cancer. 2021 June ; 2(6): 598–610. doi:10.1038/s43018-021-00203-x.

A first-in-class Polymerase Theta Inhibitor selectively targets Homologous-Recombination-Deficient Tumors

Jia Zhou[1], **Camille Gelot**[2], **Constantia Pantelidou**[3], **Adam Li**[1], **Hatice Yücel**[2], **Rachel E. Davis**[4], **Anniina Farkkila**[1], **Bose Kochupurakkal**[1], **Aleem Syed**[5], **Geoffrey I. Shapiro**[3,6], **John A. Tainer**[5], **Brian S. J. Blagg**[4], **Raphael Ceccaldi**[2,*], **Alan D. D'Andrea**[1,6,7,*]

[1]Department of Radiation Oncology, Dana-Farber Cancer Institute, Harvard Medical School, Boston, MA 02215, USA.

[2]Inserm U830, PSL Research University, Institut Curie, 75005, Paris, France.

[3]Department of Medical Oncology, Dana-Farber Cancer Institute and Department of Medicine, Harvard Medical School, Boston, Massachusetts, USA.

[4]Department of Chemistry and Biochemistry, University of Notre Dame, Notre Dame, IN 46556, USA.

[5]Departments of Cancer Biology and of Molecular and Cellular Oncology, University of Texas MD Anderson Cancer Center, Houston, TX 77030, USA.

[6]Center for DNA Damage and Repair, Dana-Farber Cancer Institute, Boston, MA, USA.

[7]Susan F. Smith Center for Women's Cancers, Dana-Farber Cancer Institute, Boston, MA, USA.

Abstract

DNA polymerase theta (POLθ) is synthetic lethal with Homologous Recombination (HR) deficiency and thus a candidate target for HR-deficient cancers. Through high-throughput small molecule screens we identified the antibiotic Novobiocin (NVB) as a specific POLθ inhibitor that selectively kills HR-deficient tumor cells *in vitro* and *in vivo*. NVB directly binds to the POLθ ATPase domain, inhibits its ATPase activity, and phenocopies POLθ depletion. NVB kills HR-

[*]**Corresponding authors:** Alan D. D'Andrea, M.D., Director, Susan F. Smith Center for Women's Cancers (SFSCWC), Director, Center for DNA Damage and Repair, Dana-Farber Cancer Institute, The Fuller-American Cancer Society Professor, Harvard Medical School, Phone: 617-632-2080, Alan_Dandrea@dfci.harvard.edu, Raphael Ceccaldi, Institut Curie, 75005, Paris, France, Phone: +33 (0)1 56 24 69 49, raphael.ceccaldi@curie.fr.

[*]These authors jointly supervised this work.

Author contributions

J.Z., R.C. and A.D.D. conceived and designed the studies. J.Z, C.G., C.P., A.L., H.Y., R.E.D., A.F., B.K., and A.S. performed experiments and analyzed data. G.I.S., J.A.T., B.S.J.B., R.C. and A.D.D. provided oversight. J.Z., R.C. and A.D.D. prepared the manuscript with input from co-authors.

Competing Interests

A.D. D'Andrea reports receiving commercial research grants from Eli Lilly & Company, Sierra Oncology, and EMD Serono and is a consultant/advisory board member for Eli Lilly & Company, Sierra Oncology, and EMD Serono. G.I. Shapiro has received research funding from Eli Lilly, Merck KGaA/EMD-Serono, Merck, and Sierra Oncology, and he has served on advisory boards for Pfizer, Eli Lilly, G1 Therapeutics, Roche, Merck KGaA/EMD-Serono, Sierra Oncology, Bicycle Therapeutics, Artios, Fusion Pharmaceuticals, Cybrexa Therapeutics, Astex, Almac, Ipsen, Bayer, Angiex, Daiichi Sankyo, Boehringer Ingelheim, ImmunoMet and Asana. The remaining authors declare no competing interests.

deficient breast and ovarian tumors in GEMM, xenograft and PDX models. Increased POLθ levels predict NVB sensitivity, and BRCA-deficient tumor cells with acquired resistance to PARP inhibitors (PARPi) are sensitive to NVB *in vitro* and *in vivo.* Mechanistically, NVB-mediated cell death in PARPi-resistant cells arises from increased double-strand break end resection, leading to accumulation of single-strand DNA intermediates and non-functional RAD51 foci. Our results demonstrate that NVB may be useful alone or in combination with PARPi in treating HR-deficient tumors, including those with acquired PARPi resistance. (151/150)

Keywords

Novobiocin; Polymerase theta (POLθ); HRD cancer; PARP inhibitor resistance; Homologous Recombination; MMEJ; Fanconi Anemia

INTRODUCTION

Deficiency of homologous recombination (HR)-mediated DNA repair occurs mainly through genetic or epigenetic inactivation of the BRCA1 and BRCA2 (BRCA1/2) genes, and it plays a role in the initiation and progression of many tumor types [1]. HR-deficiency also provides unique opportunities for targeted therapy, as exemplified by the extreme sensitivity of BRCA1/2-mutated tumors to poly (ADP-ribose) polymerase inhibitors (PARPi) [2,3]. In the last decade, several PARP inhibitors have been approved for clinical use. At first, PARPi were solely used in combination with chemotherapeutics, and platinum sensitivity was used as a surrogate marker of HR-deficiency for enrolling patients for treatment [4]. The promising clinical response of patients with germline BRCA1/2-mutations prompted the use of PARPi for patients with somatic BRCA1/2 mutations as well. In addition, it also opened up the possibility for extended use of PARPi for the treatment of various types of ovarian, breast, pancreatic and prostate tumors with HR defects [1]. PARPi efficacy is currently being evaluated in different clinical settings such as first line chemotherapy, neoadjuvant therapy (i.e. before chemotherapy), and combination therapy with chemo- or immunotherapies [1,5–8].

Despite initial sensitivity to PARPi, resistance to these drugs is emerging as the major obstacle to its clinical effectiveness in patients with HR-deficient tumors [9]. In addition, resistance to PARPi often correlates with platinum resistance, which remains the backbone therapy for most BRCA1/2-mutated tumors. The absence of alternative therapeutic options for patients with tumors with innate or acquired resistance underlines the urgency to develop additional therapeutics. While several mechanisms of PARPi resistance have been described [10–13], an effective method for overcoming such resistance is still lacking.

DNA polymerase theta (POLθ or POLQ) recently emerged as a new promising drug target for the treatment of HR-deficient tumors. POLθ expression is particularly high in subtypes of breast and ovarian tumors with defects in HR [14], where it mediates backup DNA double-strand breaks (DSBs) repair, compensating for the loss of HR [15]. As a result, POLθ is synthetic lethal with HR and POLθ inhibition in HR-deficient tumors induces cell death [14,16]. In addition, POLθ inhibition synergizes with PARPi in the killing of HR-deficient tumors [14,16].

Synthetic lethality between HR-deficiency and POLθ inhibitions hinges on several functions POLθ exhibits in maintaining genomic stability and preventing tumorigenesis [17]. POLθ was first described as a translesion DNA polymerase (TLS) [18], and this activity was recently shown to prevent the onset of skin cancer [19]. POLθ is also a crucial enzyme in the mutagenic microhomology-mediated end joining (MMEJ) repair of DSBs [20], a pathway that plays critical role in genomic stability [21]. Inhibiting PARP1, a key enzyme in MMEJ [22], prevents POLθ recruitment to sites of laser micro-irradiation [14,16]. Since POLθ inhibition and PARPi have additive effects on HR-deficient cells, these data suggest that POLθ-functions outside the PARP-mediated MMEJ are also key to the survival of HR-deficient cells.

POLθ is a large protein that contains 3 domains and is structurally and functionally distinct from other polymerases [17,23]. The N-term contains a helicase-like ATPase domain that can unwind several types of DNA structures [24], while the central domain binds RAD51, displaces RPA proteins from resected DSBs and antagonizes HR repair in an ATP-hydrolysis dependent manner [14,16,25]. Finally, the C-term contains a nuclease domain which trims DNA ends and a polymerase domain that fills in nucleotides during MMEJ [26]. Both the ATPase and polymerase domains are required for MMEJ repair [27].

POLθ has several functions that preserve genomic stability, and POLθ-mediated MMEJ repair can compensate for the loss of HR [15]. It remains unclear which of the many functions of POLθ underlies the synthetic lethality with HR. Nevertheless, POLθ exhibits unique features of druggability, providing a strong rationale for developing POLθ inhibitors [4,28].

Here, we performed a small-molecule screen for inhibitors of POLθ ATPase activity and identified the antibiotic novobiocin (NVB) as a specific and potent inhibitor of human POLθ. NVB binds to purified POLθ protein, prevents its recruitment to DNA damage, and inhibits MMEJ repair. Importantly, we show that NVB selectively kills HR-deficient (BRCA1- and BRCA2-deficient) cells over wild-type cells and potentiates the cytotoxic effect of PARPi in HR-deficient tumor cells *in vitro* and *in vivo*. Moreover, NVB also kills HR-deficient, PARPi-resistant tumor cells. Our results demonstrate that NVB can be used alone or in combination with PARPi for treating HR-deficient tumors, even after they have acquired PARPi resistance.

RESULTS

A small-molecule screen identifies NVB as a specific POLθ inhibitor

The ATPase activity of POLθ is required for the survival of HR-deficient cells [14]. We took advantage of the strong *in vitro* ATPase activity of purified POLθ (Extended Data Fig. 1a) and performed a large-scale small-molecule screen to identify POLθ inhibitors based on the ADP-Glo luminescent assay (Fig. 1a,b). We screened a total of 23,513 small-molecules across multiple libraries (enriched with known bioactive compounds, Supplementary Tables 1–2) in duplicate, and identified 72 compounds that significantly (z-score < −4) reduced POLθ ATPase activity (Fig. 1b, Supplementary Table 3). These compounds account for only 0.3% of the total small-molecules screened, arguing for a low rate of false-positive hits. A secondary screen using the 72 initial hits was performed in the presence and absence of

ssDNA, in order to confirm the initial screen results and to exclude compounds that directly interact with ssDNA (Extended Data Fig. 1b). Among the 72 small molecules, 10 hits were identified to have inhibited POLθ ATPase more than 50% both with and without ssDNA (≤15% difference in inhibition) (Supplementary Table 4). Aurintricarboxylic acid (ATA), reactive Blue 2 (RB), suramin (SUR), and novobiocin (NVB) were the four most potent POLθ inhibitors.

These top hits were individually verified in a ^{32}P-based radiometric ATPase assay with POLθ and another known DNA repair-related ATPases SMARCAL1 [29]. Only NVB showed high specific inhibition of POLθ with little effect on SMARCAL1, while other compounds inhibited both ATPases (Extended Data Fig. 1c). We thus focused our future studies on novobiocin. Next, we performed a dose response of NVB on POLθ ATPase activity using ADP-Glo assay, along with six other DNA repair related enzymes HSP90AA1, TRIP13, BLM, RAD51, SMARCAL1 and CHD1 (Fig. 1c and Extended Data Fig. 1d). Novobiocin inhibited POLθ with an IC50 of 24 μM, but it did not significantly inhibit other ATPases, supporting the specificity inhibition of novobiocin on POLθ.

To further evaluate the specificity of novobiocin (NVB) for POLθ, we analyzed its binding capacity. NVB-conjugated beads pulled down the purified ATPase domain of POLθ, but not purified SMARCAL1, CHD1, BLM, and RAD51, suggesting that NVB directly and specifically binds to the POLθ ATPase domain *in vitro* (Extended Data Fig. 1d–f). NVB-conjugated beads also pulled down POLθ-GFP expressed in cells, and this binding was competed by free NVB (Extended Data Fig. 1g–h). Thermal shift assays using cell lysate of GFP-POLθ expressing HEK293T cells showed that NVB stabilized GFP-POLθ (Extended Data Fig. 1i). Thermal shift assays with purified POLθ-ATPase domain showed that NVB increased POLθ stability in a dose dependent manner, further suggesting a direct ligand-protein binding of NVB to POLθ (Extended Data Fig. 1j). As controls, NVB did not increase the thermal stability of BLM or MRE11 (Extended Data Fig. 1k–l). Finally, we performed molecular docking to identify the NVB binding site using the published crystal structure of POLθ ATPase domain [30]. The computational docking results revealed a deep tunnel within the POLθ ATPase domain that could accommodate NVB, which is located next to the ATP binding pocket (Fig. 1d). Taken together, these data demonstrate that NVB binds directly and specifically to the POLθ ATPase domain *in vitro*.

We next assessed whether cellular exposure to NVB has the same consequences as POLθ depletion. Both the ATPase and the polymerase domains contribute to efficient MMEJ repair activity [27], and the PARP-dependent recruitment of POLθ to DSB sites is a crucial step in this function [14,16]. Phenocopying the ATPase mutant of POLθ, inhibition of POLθ by NVB prevented the recruitment of POLθ to laser micro-irradiated DNA damage sites in human cells (Fig. 1e). Consequently, NVB inhibited the MMEJ activity in U2OS cells, as measured by the GFP-based EJ2 repair assay, but it had little effect on HR activity measured by the DR-GFP reporter assay (Fig. 1f). POLθ also functions as an anti-recombinase that antagonizes HR, and depletion of POLθ increases RAD51 [14] and γH2AX [31] foci assembly. Similarly, more RAD51 foci and γH2AX foci were observed after IR in the presence of NVB in U2OS cells (Extended Data Fig. 2a–b), although the effect was not as strong as previously reported with siRNA POLθ knockdown [14]. Taken together, these results establish

that NVB-mediated POLθ inhibition impairs POLθ DNA repair function and phenocopies POLθ depletion in human cells.

NVB specifically Kills HR-deficient tumors

NVB is a safe drug and has already been used in anti-cancer trials, although the treated patients were not preselected to have HR-deficient cancers [32–35]. Since depletion of POLθ is synthetically lethal in HR-deficient tumor cells [14,16], we next directly tested whether NVB can kill HR-deficient tumor cells in animal models. First, we evaluated the efficacy of NVB in tumors derived from the K14-Cre-*Brca1*$^{f/f}$;*Trp53*$^{f/f}$ genetically-engineered mouse model (GEMM) of triple-negative breast cancer (TNBC) [36,37]. Tumors from this model were transplanted into immunocompetent FVB/129P2 syngeneic mice that were subsequently treated with NVB. NVB strongly suppressed the growth of these *Brca1*-deficient GEMM-derived tumors (Fig. 1g and Extended Data Fig. 3a). The NVB-treated tumors were significantly smaller compared to the vehicle-treated after 7 days of treatment and beyond. NVB prolonged the overall survival of the tumor-bearing mice by 3-fold compared to vehicle, with median survival times of 29 and 10 days for NVB- and vehicle-treated mice, respectively (Fig. 1h).

Next, we tested whether the efficacy of NVB *in vivo* was specific to HR-deficient tumors. *FANCF*-deficient TOV21G cells are human ovarian cancer cells with reduced HR capacity, which grow well as tumor xenografts in mice [38,39]. We thus performed a mouse xenograft study with the FANCF-deficient (TOV21G + empty vector) and the FANCF-complemented (TOV21G + FANCF cDNA) cell lines (Fig. 2a,b). *In vitro*, TOV21G + EV cells but not TOV21G + FANCF cDNA cells were sensitive to olaparib and NVB (Extended Data Fig. 3b,c) [39]. *In vivo*, while vehicle treatment had no impact on the growth of FANCF-deficient or FANCF-complemented tumors, NVB specifically impaired the growth of the FANCF-deficient tumors, with no effect on FANCF-complemented tumors (Fig. 2a,b). We also measured RAD51 foci as a pharmacodynamic biomarker and showed that RAD51 foci were strongly induced in the treated tumors (Extended Data Fig. 3d–f). These results demonstrate that NVB strongly and specifically suppresses the growth of HR-deficient tumors *in vivo*.

To confirm and strengthen the *in vivo* results, we studied isogenic pairs of HR-deficient and HR-proficient cells *in vitro*. We generated *BRCA1* and *BRCA2* knockout RPE1 cells (referred as *BRCA1*$^{-/-}$ and *BRCA2*$^{-/-}$) in a *TP53*$^{-/-}$ background, which were sensitive to PARPi (Extended Data Fig. 4a,b). Consistent with our *in vivo* data, clonogenic survival assays showed that NVB significantly reduced the survival of *BRCA1*$^{-/-}$ and *BRCA2*$^{-/-}$ cells, compared to the isogenic WT cells (Fig. 2c and Extended Data Fig. 4c). We also tested the top initial hits from our screen for their ability to differentially affect the survival of *BRCA1*$^{-/-}$ and WT cells. Among those, NVB had the highest efficacy in selectively killing the *BRCA1*$^{-/-}$ cells (Extended Data Fig. 4d).

To demonstrate the cellular outcome of NVB exposure, we next showed that NVB exposure induces apoptosis in *BRCA1*$^{-/-}$ but not WT cells in a dose dependent manner (Extended Data Fig. 5a). NVB induced chromosomal aberrations and radial chromosomes (a marker of genomic instability) in *BRCA1*$^{-/-}$ cells, even in the absence of the crosslinking agent mitomycin C (MMC) (Extended Data Fig. 5b–d), confirming that NVB increases DNA

damage. These results further demonstrate that NVB phenocopies POLθ depletion, and they indicate that NVB-mediated POLθ inhibition is synthetically lethal with HR deficiency and specifically induces cell death in HR-deficient tumor cells.

POLθ is the major target of NVB in human cells

Off target effects are major concerns of biological small inhibitors. To further evaluate whether POLθ is the specific target of NVB and to demonstrate the specificity of NVB in cells, we knocked out the *POLQ* gene in RPE1 cells using CRISPR-Cas9 and asked whether loss of *POLQ* alleviates the cytotoxicity of NVB. *POLQ* knockout cells were confirmed by genomic sequencing and their increased sensitivity to irradiation (Fig. 2d). Importantly, RPE1 $POLQ^{-/-}$ cells showed increased tolerance to NVB compared to the WT cells (Fig. 2e). In addition, $POLQ^{-/-}$ U2OS cells were also more resistant to NVB than WT cells (Extended Data Fig. 6a–e). These data indicate that POLθ is a major target of NVB in human cells.

NVB is a known coumarin antibiotic that inhibits DNA gyrase in bacteria [40]. NVB has been reported to inhibit the ATPase of HSP90 and of the DNA gyrase homolog topoisomerase II (TOP2) in eukaryotes [41,42], suggesting that these enzymes may be off-target enzymes of NVB. However, other reports suggest that NVB does not inhibit TOP2 in eukaryotic cells [43]. Additionally, the reported IC_{50} of these targets are very high (approximately 700 μM for HSP90 and 300 μM for TOP2), compared with the IC_{50} of POLθ (24 μM by ATPase inhibition assay, Fig. 1c). Nevertheless, we next examined whether the cytotoxic effect of NVB in HR-deficient cells resulted from off-target inhibition of HSP90 or TOP2. Unlike the well-characterized HSP90 inhibitor PU-H71, NVB treatment at a concentration that killed HR-deficient cells (i.e. 100 μM) did not induce the degradation of HSP90 clients such as AKT1, BRCA1, or CDK6, or increase the expression of HSP70 (Extended Data Fig. 7a–c). These results suggest that the cytotoxic effect of NVB is not related to HSP90 inhibition. Furthermore, the combination of NVB and the TOP2 inhibitor etoposide exhibited additive cytotoxicity in TOV21G and CAPAN1 cells (Extended Data Fig. 7d,e), suggesting that NVB and etoposide do not share TOP2 as a target and that NVB cytotoxicity is unrelated to TOP2 inhibition.

NVB potentiates the effect of PARPi in HR-deficient tumors

PARPi are currently being evaluated in different combination therapy settings with cytotoxic chemotherapy, radiation, targeted therapies, and immunotherapies [44]. We explored whether the combination of NVB and a PARPi may be more effective than PARP inhibition alone in killing HR-deficient tumors. Indeed, NVB further sensitized $BRCA1^{-/-}$ RPE1 cells to the PARPi rucaparib, but not BRCA-proficient WT cells in clonogenic assays (Fig. 2f). We studied the combination with a second PARPi, olaparib, where synergism of NVB and olaparib was also observed in HR-deficient TOV21G + EV cells, but not in HR-proficient TOV21G + FANCF cells (Extended Data Fig. 7f). Importantly, NVB reduced the IC_{50} of rucaparib by more than 20-fold in $BRCA1^{-/-}$ RPE1 cells and the IC_{50} of olaparib more than 40-fold in TOV21G cells compared to their respective HR-proficient counterparts (Fig. 2f and Extended Data Fig. 7g). One strategy to prevent acquired resistance during treatment is

combination therapy. The observed synergy between NVB and PARPi prompted us to evaluate whether NVB could overcome PARPi resistance in HR-deficient tumors.

POLθ inhibition by NVB overcomes acquired PARPi resistance

Multiple PARP inhibitors (PARPi) including olaparib, niraparib, rucaparib, and talazoparib have received approval for the treatment of ovarian and breast tumors with HR deficiency [45]. Despite the remarkable initial tumor response and improved progression-free survival (PFS) in HR-deficient patients [5–8], acquired PARPi resistance is emerging as an unmet medical need [9].

To evaluate whether POLθ inhibition could represent a novel therapeutic option for PARPi-resistant tumors, we first tested the efficacy *in vivo* of NVB in the patient-derived xenograft (PDX) model DF83, generated from an HR-deficient (loss of RAD51C expression), human high-grade serous ovarian carcinoma [46]. NSG mice bearing the HR-deficient DF83 ovarian cancer PDX model were treated with olaparib, NVB, or a combination of the two, and tumor growth was monitored by bioluminescence imaging (BLI) (Fig. 3a). In order to determine the combined effect with NVB, olaparib was delivered at a submaximal dose (50 mg/kg daily), and we observed only a small degree of tumor growth inhibition. Treatment of DF83 with NVB alone (75 mg/kg, twice a day) led to tumor regression, while tumors in vehicle-treated mice showed exponential growth (Fig. 3b). Strikingly, when the DF83 tumor-bearing mice were given NVB and olaparib in combination, we observed complete tumor regression, and few tumor cells were detectable via BLI on day 28 in this group (Fig. 3a,b). These *in vivo* results suggest NVB may be useful in combination with PARPi to achieve better efficacy and prevent drug resistance in HR-deficient tumors. No significant toxicity to normal mouse tissue was observed from the drug combination.

Next, we evaluated the efficacy of NVB alone and in combination with olaparib in the PARPi-resistant PDX model DF59, which was isolated from a patient with a germline *BRCA1* mutation and acquired PARPi resistance. This model harbors biallelic mutations in the *TP53BP1* locus, providing a mechanism of the acquired PARPi resistance [46]. In the DF59 PDX model, there was no response to olaparib monotherapy, but NVB monotherapy substantially reduced tumor growth, indicating a lack of cross-resistance between PARP inhibition and NVB. Importantly, the combination of NVB and olaparib further inhibited DF59 tumor growth, with tumor regression in the first two weeks (Fig. 3c,d). In contrast to DF83 and DF59 models, the BRCA1 WT, HR proficient PDX model DF149 was resistant to both drugs and to the combination (Fig. 3e,f). These data demonstrate that NVB can inhibit the growth of a *BRCA1*-mutated, PARPi-resistant tumors *in vivo* and that the combination of NVB and a PARPi is particularly effective in treating at least some PARPi-resistant tumors.

NVB induces excessive DSB end resection and RAD51 foci

We next studied the mechanism of cell killing by NVB. Previous studies demonstrated that the ATPase domain of POLθ counteracts RPA binding at resected DSBs to facilitate their repair by MMEJ [25]. We therefore hypothesized that DSBs will be excessively resected when POLθ is inhibited. We measured DNA resection at DSBs, generated by AsiSI, in U2OS cells

in the presence or absence of NVB. In this assay, DSBs were induced by 4-hydroxy-tamoxifen (4-OHT), and the percentage of single-stranded DNA (ssDNA) was measured by qPCR [47]. The amount of ssDNA around the DSB was significantly higher when cells were treated with NVB versus DMSO (Fig. 4a). Consistent with this result, NVB-treated tumor samples from the DF59 PDX model exhibited higher levels of phospho-RPA32 (p-RPA32), a measure of ssDNA accumulation, compared to vehicle-treated samples (Fig. 4b). These data suggest that POLθ inhibition by NVB can promote DSB end resection.

We previously showed that depletion of POLθ in HR-deficient tumors causes RAD51 accumulation [14], perhaps resulting from excessive DSB end resection. Similarly, 53BP1 and POLθ are synthetic lethal, and 53BP1/POLθ double knockout cells also have increased end resection and elevated RAD51 accumulation [48]. We reasoned that NVB may induce non-functional RAD51 foci in HR-deficient tumors with PARPi resistance *in vivo*. To test this hypothesis, we collected tumor cells from the PARPi and/or NVB treated PDX models and evaluated RAD51 foci by immunohistochemistry (Fig. 4c). Since DF83 is an HR-deficient and PARPi sensitive model, RAD51 foci were not observed. The HR-restored and PARPi-resistant DF59 model, with biallelic 53BP1 mutations, exhibited a strong increase in RAD51 staining when treated with NVB alone or in combination with olaparib (Fig. 4c,d). Similarly, TOV21G xenograft tumors exhibited increased RAD51 foci by immunohistochemistry *in vivo* after NVB treatment, which was further enhanced by olaparib (Extended Data Fig. 3d–f). Next, we evaluated the effect of NVB on a PARPi resistant clone (MDA-MB-436-R) of the BRCA1-mutated breast cancer cell line MDA-MB-436 [49]. Like the DF59 PDX model, this resistant cell line restored HR by two mechanisms, namely the stabilization of mutant BRCA1 protein and the loss of 53BP1. While highly resistant to olaparib, the MDA-MB-436-R cells were sensitive to NVB similarly to the parental cells (Fig. 4e,f). Importantly, NVB induced RAD51 accumulation in MDA-MB-436-R cells but not in the parental cells (Fig. 4g). Since the parental and MDA-MB-436-R cells are both sensitive to NVB, the elevated RAD51 levels appear to be non-functional for HR, consistent with the increased resection observed in the presence of NVB. Taken together, our data suggest that the elevated DSB end resection, as well as the subsequent accumulation of ssDNA intermediates and non-functional RAD51 loading, are a plausible mechanism of cell killing by NVB in PARPi resistant HR-deficient tumor cells (Fig. 4h).

NVB overcomes multiple PARPi resistance mechanisms

To better understand the mechanism by which NVB overcomes PARPi resistance, we generated several PARPi-resistant clones from *BRCA1*$^{-/-}$ *RPE1* cells by gradually exposing them to increasing concentrations of PARPi (Fig. 5a). We selected four clones (named R1 to R4), all of which have acquired resistance to olaparib (Extended Data Fig. 8a–c). Multiple PARPi resistance mechanisms were identified in these clones, corresponding to published mechanisms [9]. Replication fork stabilization was evident in the R1 and R2 clones (Extended Data Fig. 8d). The R1, R3, and R4 clones have restored RAD51 foci, suggesting restored HR activity in these clones (Extended Data Fig. 8e). The restoration of HR repair in these clones may have resulted in part from their downregulation of the Shieldin complex and subsequent downregulation of NHEJ repair. Indeed, the R3 clone had decreased expression of REV7, a component of the Shieldin complex, and the R4 clone had decreased 53BP1

expression (Extended Data Fig. 8f–g). None of the clones had re-expressed BRCA1, thereby excluding somatic reversion of BRCA1 as an underlying PARPi resistance mechanism (Fig. 5b and Extended Data Fig. 8h). Strikingly, all four PARPi-resistant clones remained sensitive to NVB to a similar extent as the parental RPE-*BRCA1*$^{-/-}$ cells (Fig. 5c,d), suggesting that NVB may overcome multiple mechanisms of acquired resistance to PARPi. To demonstrate that genetic inhibition of POLθ also causes cell death in the PARPi-resistant *BRCA1*$^{-/-}$ clones, we depleted POLθ in R1, R2, and the parental cells and measured their cell survival. Upon POLθ depletion, the parental *BRCA1*$^{-/-}$ cells and the PARPi-resistant clones, but not WT RPE1 cells, showed reduced survival, suggesting that POLθ inhibition was the mechanism for NVB cytotoxicity in those cells (Extended Data Fig. 8i).

We also examined more clinically relevant PARPi-resistant, HR-deficient models, using tumor cells derived from patients. MDA-MB-436-R cells, with stabilized mutant BRCA1 protein and loss of 53BP1, were NVB sensitive (Fig. 4e,f). In addition, we studied the PARPi-resistant clone UWB1.289-YSR12 (derived from the *BRCA1*-null human ovarian cancer cell line UWB1.289), which acquired resistance to PARPi via stabilization of replication forks [50]. These cells also remained sensitive to NVB, although they are highly resistant to olaparib (Extended Data Fig. 9a–b), again suggesting that acquired resistance to PARPi does not determine cross-resistance to NVB. Taken together, these data show that NVB may overcome multiple mechanisms of acquired resistance to PARPi.

POLθ expression is a predictive biomarker for NVB sensitivity

POLθ mRNA expression is increased in HR-deficient tumors and in several other cancers associated with poor prognosis [14,51]. We asked whether increased POLθ mRNA and protein expression may serve as a predictive biomarker for NVB sensitivity. As expected, CRISPR-mediated knockout of *BRCA1* in RPE-1 cells resulted in increased POLθ expression as compare to the parental cells (Fig. 5e and Extended Data Fig. 9c). Interestingly, all selected PARPi-resistant clones (R1-R4) retain high POLθ expression, revealing a direct correlation between POLθ expression and NVB sensitivity (Fig. 5e). This correlation was also present in the BRCA1-deficient MDA-MB-436 cells. MDA-MB-436-R cells with acquired PARPi-resistance exhibited elevated POLθ mRNA expression and retained NVB sensitivity, while complementation of the parental cells with WT BRCA1 cDNA decreased POLθ expression and NVB sensitivity (Fig. 5f). The direct correlation of POLθ expression and NVB sensitivity was further observed in the HR-deficient PDX models, where the elevated POLθ expression in DF83 and DF59 correlated with their high sensitivity to NVB *in vivo* (Fig. 5g and Fig. 3a–f).

Another known mechanism of PARPi resistance in *BRCA1/2*$^{-/-}$ tumors in the clinic is somatic reversion of the BRCA1/2 genes [4]. We determined whether NVB could overcome PARPi resistance caused by BRCA2 reversion. Unlike other PARPi resistant cells we analyzed, BRCA2-deficient tumor cells with near-perfect somatic reversion or CRISPR-edited reversion of BRCA2 (PEO4 and CAPAN1-CR) [10,52] were not only resistant to PARPi but also to NVB, when compared to their HR-deficient parental cell lines (PEO1 and CAPAN1) (Fig. 5h–i and Extended Data Fig. 9d–e). These data suggest that NVB can overcome some but not all mechanisms of PARPi resistance. Importantly, the low POLθ

expression was a predictive biomarker for NVB resistance. For the PARPi-resistant cell lines with BRCA2 reversion mutations (PEO4 and CAPAN1-CR), their resistance to NVB correlated with their low POLθ protein expression levels by Western blot (Fig. 5j and Extended Data Fig. 9f). The resistance of the DF149 PDX model *in vivo* correlated with its low POLθ expression (Fig. 5g). Also, the loss of POLθ in RPE1 cells correlated with resistance to NVB (Fig. 2e). Taken together, in all cases we examined, POLθ expression level correlated with cellular sensitivity to NVB, suggesting that POLθ expression in a tumor biopsy could provide a convenient predictive biomarker for patient enrollment in future clinical trials with NVB or other POLθ inhibitors.

DISCUSSION

In summary, NVB is a specific and potent POLθ inhibitor which phenocopies POLθ depletion and is synthetic lethal in HR-deficient tumors. In the clinic, many tumors with acquired PARPi resistance are likely to remain sensitive to NVB, depending on their mechanism of resistance. Tumors which acquire PARPi resistance by downregulating NHEJ and partially restoring HR repair remain sensitive to NVB. For these tumors, the persistent high level of POLθ expression is a predictive biomarker for their NVB responsiveness, and the NVB-induced RAD51 accumulation provides a convenient pharmacodynamic biomarker for clinical trials.

Our work provides mechanistic insights into the cause of synthetic lethality induced by NVB. BRCA1/2-deficient, HR defective tumor cells are hyperdependent on POLθ, which is recruited for MMEJ by PARP at DSBs and by XRCC1 along with MRE11 at replication forks [14,53]. Accordingly, NVB kills these HR-deficient cells by blocking the tumor-critical MMEJ activity of POLθ. On the other hand, BRCA1/2-deficient tumor cells which have acquired PARPi resistance, resulting from the downregulation of 53BP1 or other Shieldin components, appear to require POLθ activity for limiting end resection. Accordingly, NVB kills these tumor cells by enhancing end resection, leading to toxic levels of ssDNA intermediates and non-functional RAD51 loading.

Finally, our findings may translate to a potential new therapy for treating HR-deficient tumors in addition to PARP inhibition. Importantly, NVB is an oral and well-tolerated drug, and it has previously been investigated in Phase 1 cancer trials [32–35]. Some partial responses were documented, even though the enrolled patients were not preselected to have HR-deficient cancers [32]. Other previous clinical studies have shown that the serum concentration at which NVB specifically kills HR-deficient cells (*i.e.* 100 μM) is readily achievable without causing adverse side effects in humans [33–35]. In addition, the half-life of NVB in humans (6.0 hours) is significantly longer than the half-life in mice (82 minutes) [32], suggesting that NVB may be even more efficacious in humans than in our mouse models. In summary, results in this study provide a strong rationale for future clinical studies of NVB alone or in combination with PARPi to prevent or overcome PARPi resistance.

METHODS

Compounds, inhibitors and antibodies

Chemical compounds, including PARP inhibitors Olaparib (#S1060) and Rucaparib (#S1098), Novobiocin (#S2492), etoposide (#S1225), and PU-H71 (#S8039) were purchased from Selleckchem. Chemicals were dissolved in DMSO and kept in small aliquots at −80°C. The key sources of antibodies are: POLθ (Sigma #SAB1402530), γH2AX (Millipore #05–636), RAD51 (Santa Cruz Biotechnology, SCB, #sc-8349), CDK6 (SCB, #sc-7961), AKT1 (SCB #sc-5298), HSP70 (SCB #sc-24), HSP90 (SCB #sc-13119), and FANCF (Everest Biotech, #EB06112).

Protein purification

A POLθ fragment (ΔPol) containing the ATPase domain with a RAD51 binding site (amino acids 1 to 987) was cloned into pFastBac-C-Flag and purified from baculovirus-infected SF9 insect cells. POLθ expressing cells were lysed in lysis buffer (500 mM NaCl, 0.01 % NP-40, 0.2 mM EDTA, 20% Glycerol, 1 mM DTT, 0.2 mM PMSF, 20 mM Tris [pH 7.6]) supplemented with Halt protease inhibitor cocktail (Thermo Fisher) and Calpain I inhibitor (Roche). The cell lysates were incubated with M2 Flag beads (Sigma) for 3 hours at 4 ^{o}C on a spinning wheel. The beads were washed 3 times lysis buffer and protein was then eluted in lysis buffer supplemented with 0.2 mg/ml of Flag peptide (Sigma). The protein was then concentrated in lysis buffer using 10 kDa centrifugal filters (Amicon). SMARCAL1, CHD1, BLM, RAD51 and TRIP13 were purified in house using similar protocol. BLM-ATPase domain and MRE11-catalytic domains were purified by affinity followed by gel-filtration chromatography. Purified HSP90AA1 protein was purchased from Abcam (ab78425).

High throughput small Molecule screen

The ATPase activity based high throughput small-molecule screen was performed at ICCB Longwood Screen Facility at Harvard Medical School. On the day of screening, Combi machine was used to dispense 10 μl aliquots of a master mix containing 600 nM of 30-mer single-stranded DNA substrate and 10 nM of POLθ protein (ΔPol) into each well of a 384 well plate (Corning 3820). Small molecules were added to wells in the 384 well plates by Seiko Pin transfer robot. Plates were covered with aluminum seals and spun down at 1000 rpm and sat for 1 hour to allow small molecules to bind protein. 3 μL of 433.33 μM ultra-pure ATP was added to every well except no-substrate control wells. Plates were stored overnight (16 hours) in a humidified plastic chamber. Next day, 6.5 μL of ADP-Glo reagent (Promega) was added to every well using the Combi machine. After one-hour incubation, 13 μL of Kinase Detection Reagent (Promega) was added to every well and incubated for another hour. Data was collected using the Envision plate reader by measuring luminescence signal. More information about the screen is available in Supplementary table 1.

Statistical Analysis of the high throughput screen

The inhibition strength of screened compounds was evaluated using Z-score analysis. Since most compounds did not affect POLθ-ATPase activity, data for all compounds was used to calculate plate mean (μ) and standard deviation (σ). Every compound is then assigned a Z-

score using the equation $z = (x – \mu) / \sigma$. Percentage inhibition analysis. Percentage inhibition of compounds was determined by normalizing to the DMSO control. Wells with DMSO were averaged to find the average signal without inhibitor, and a different DMSO average was calculated for each plate. The % activity was calculate using the following formula: % activity = [(signal with compound) / (average signal with DMSO)] x 100%.

ATPase activity assay

The ATPase activity of POLθ was measured using the ADP-Glo kinase assay (Promega). Reactions were done in 50 μl of reaction buffer (40 mM Tris-HCl buffer (pH 7.6), 20 mM $MgCl_2$, 0.1 mg/ml BSA, and 1 mM DTT) in black 96 well plates. The final concentrations were 600 nM of 30mer single-stranded DNA, 50 nM of purified POLθ-ΔPol protein, and 100 μM of ATP, with DMSO or NVB. The sequence of the 30mer ssDNA used in the assay was: 5'-CCAGTGAATTGTTGCTCGGTACCTGCTAAC-3'. The order for adding the components were: 10 μl 1x reaction buffer, 10 μl of 10x ssDNA, 10 μl of 10x POLθ, 10 μl of 10x NVB or DMSO (incubate at room temp for 15 min), and finally 10 μl of 10x ATP, and all components were prepared in 1x reaction buffer. DMSO wells represented 0% inhibition while no-enzyme wells represented 100% inhibition. Plates were covered with an aluminum seal and incubated at room temperature overnight (16 hours). The following day, 50 μl of ADP-Glo reagent (Promega kit) was added to each reaction well and incubated at room temp for one hour. Next, 100 μl of Kinase detection reagent (Promega kit) was added to the wells, and plates were incubated for another hour. Finally, ATP hydrolysis was quantified by luminescence measured on a plate reader. Measurement of other ATPases were done using the same conditions and protocol. In some cases as indicated, ^{32}P-based ATPase activity assay was also performed as previously described [54].

Thermal Stability Assays (TSA)

POLθ helicase domain was expressed using POLQ-A construct (Addgene#74645) in HF insect cells and purified as described previously [30]. Thermal stability of POLθ helicase domain in the presence of NVB was measured using Prometheus with NanoDSF (NanoTemper). Given that the intrinsic fluorescence emission from the protein coincide with the chromophore core in the NVB, we monitored scattering to measure the protein stability with temperature. POLθ helicase domain (0.5 mg/ml in 25 mM HEPES (pH=8) and 200 mM NaCl) was incubated with indicated concentration of NVB for 30 minutes before the sample was loaded into capillaries for the scattering measurement with increasing temperature at 1 °C/minute starting from 25 °C till 90 °C. Shift in the peak max of scattering was estimated from the first derivative of the scattering data. All data points were an average from three replicates and plotted in GraphPad Prism8.

Preparation of Novobiocin–Sepharose 6B Beads

NVB–Sepharose 6B Beads were prepared similarly as previously described [55]. 0.5 gram of epoxy-activated Sepharose 6B (Sigma-Aldrich E6754) was washed thoroughly and swollen in 50 mL of distilled water for 1 hour at room temperature. The resin was washed once with coupling buffer (0.3 M Sodium Carbonate [pH 9.5]). The washed resin was mixed with 500 mg of NVB in 50 mL of coupling buffer and incubated at 37 °C with rotation overnight. Next day, the resin was washed with coupling buffer three times to remove excess NVB. The

remaining epoxy-active groups were blocked with 1 M ethanolamine (in coupling buffer) for 6 hours at 37 °C with gentle rotation. The beads were sequentially washed with coupling buffer, 0.5 M NaCl in coupling buffer, distilled water, 0.5 M NaCl in 0.1 M sodium acetate (pH 4), and twice in distilled water. The beads were re-suspended and stored in 25 mM HEPES (pH 7.6), 200 mM KCl, 10% ethylene glycol, and 1 mM EDTA.

GFP reporter-based DNA repair assays

U2OS cells containing the DR-GFP (for HR) and EJ-2 (for MMEJ) repair substrates were gifts from Dr. Jeremy Stark at Beckman Research Institute of the City of Hope. To measure the repair efficiency, 1×10^5 cells were plated in each well of a 12-well plate. Indicated compounds or DMSO were added to the medium for 24 hours, and cells were infected with Adenoviruses expressing the I-SceI enzyme. Two days after infection, cells were trypsinized and GFP-positive cells were quantified by flow cytometry (Beckman).

RAD51 and γH2AX focus formation assay

Cells were pre-treated with DMSO or NVB for 24 hours before receiving 5 Gy of irradiation. 4–8 hours after irradiation, cells were extracted and fixed with 1% PFA, 0.5% methanol, and 0.5% TritonX-100 in PBS for 20 min at room temperature on a shaker. Fixed cells were washed with PBS twice and blocked with BTG buffer (1 mg/mL BSA, 0.5% TritonX-100, and 3% of goat serum, 1 mM EDTA) for 1 hour. Cells were then incubated with a rabbit Rad51 antibody (Santa Cruz Technology sc-8349 or Cell Signaling Technology #8875) and mouse γH2AX antibody (Millipore #05–636) in BTG buffer. After wash with PBS three time, cells were incubated with Alexa-488 (Life Technologies A11034) or Alexa-594 (Life Technologies A11005) conjugated secondary antibodies in BTG buffer for 1 hour. The dishes were washed with BTG buffer once and PBS twice, and mounted with mounting solution with DAPI for immunofluorescence microscopy. Images of random fields were taken under a 63x oil lens. Foci were visualized and quantified using ImageJ software. Images were prepared in the Zen software v3.1 (Zeiss, blue edition).

CellTiter-Glo (CTG) cell viability assay

The CellTiter-Glo luminescent cell viability assay kit (Promega #G7573) was used to measure cell viability after drug treatment. The CellTiter-Glo kit determines the number of viable cells in culture based on quantitation of the ATP present, an indicator of metabolically active cells. 500 to 1000 cells per well were seeded in a 96-well plate in 100 μL media volume. 24 hours later, cells were treated with indicated drugs by adding 100 μL medium containing 2x concentrated drug of desired final concentration. Cells were cultured in drug containing medium for 6 days, by then cell viability was determined by measuring the luminescent signal, following the manufacturer's instructions. Survival fraction of drug-treated cells was normalized to DMSO-treated control. Survival, IC50 and statistics were determined by using the GraphPad Prism software.

Clonogenic survival assay

Cells were seeded, at 2 different concentrations, into each well of a 6-well plate (100 and 200 cells for WT RPE1; 500 and 1000 cells for HR-deficient cells). Next day, cells were

treated with the indicated doses of inhibitors. For combination studies, cells were treated first with Novobiocin or DMSO for 24h, washout and then incubated in fresh media containing Novobiocin or DMSO with increasing concentration of PARPi. Cells were allowed to grow in drug-containing medium for 12 to 14 days. Cells were fixed and stained with 0.2% crystal violet in methanol for 30 min (Crystal Violet solution, Sigma HT90132), and rinsed with distilled water three times. The stained dishes were air-dried, and the number of colonies (>50 cells) was counted in each well. Surviving fraction was plotted for each drug concentration by normalizing them to the untreated cells.

Gene knockouts and cell line generation

BRCA1, BRCA2 and POLQ knockouts were generated in RPE-1 cells in which TP53 has been first knocked out (RPE1- P53$^{-/-}$). BRCA1 knockout were previously generated in RPE1-TP53$^{-/-}$ (named here RPE.1a) in Alan d'Andrea's laboratory (DFCI) [56]. BRCA2 and POLQ knockouts were generated in Raphael Ceccaldi's laboratory (Institut Curie) using another clone of RPE1-TP53$^{-/-}$ (named here RPE.1b). Accordingly, we named the following knockouts: RPE1a BRCA1$^{-/-}$ and RPE1b POLQ$^{-/-}$, RPE1b BRCA2$^{-/-}$. Knockouts were generated by co-transfection of Cas9 (pSpCas9(BB)-2A-GFP Addgene #48138) (PX458) and sgRNA vectors (gRNA cloning vector Plasmid Addgene #41824) by Lipofectamine LTX with Plus Reagent (Thermo Fisher). After subcloning into 96 wells plate, single colonies were screened by PCR. Briefly, DNA was extracted by adding 30 µl of a 50 mM NaOH solution per well after which the plate was put at 95°C for 10 minutes. Then, 2.5 µl of 1M Tris-HCL PH 7.5 was added per well and 2 µl of the extracted DNA was used to perform screening PCR (Terra PCR Direct Polymerase, Takara Clontech). Clones were selected for the presence of deletion PCR band and absence of 5' and 3' junction PCR band. RPE1b cells were obtained using the TP53 sgRNA sequence: GGCAGCTACGGTTTCCGTC. RPE1b BRCA2$^{-/-}$ cells and RPE1b POLQ$^{-/-}$ were obtained using two sgRNA vectors targeting introns flanking exon 2 of the *BRCA2* gene: BRCA2–2: GGTAAAACTCAGAAGCGC; BRCA2–3: GCAACACTGTGACGTACT or the POLQ gene: POLQ-2: GGAAGGCTTTTAGGTCAGTA; POLQ-3: GGCAACGGGGGCAGCTCCGC. PCR primer sequences used for genotyping BRCA2 knockout were the following: deletion PCR (seqBRCA2-For: GCTGTATTCCGAAGACATGCTGATGG; seqBRCA2-Rev: TTGTTCCTACTGCTAGTCAAGGG), 5' Junction PCR (seqBRCA2-For + exon2-Rev: TACCTACGATATTCCTCCAATGCTT), 3' Junction PCR (seqBRCA2-Rev + exon2-For: AAGCATTGGAGGAATATCGTAGGTA). For genotyping POLQ knockout we used: deletion PCR (seqPOLQ-For: GAAGAGCTACTTCCCTGATCTACC; seqPOLQ-Rev: CCCAACCAATCTCATTACGAATCC), 5' Junction PCR (seqPOLQ-For + exon2-Rev: GAGCCTGATTCTGAACGCCGCCG), 3' Junction PCR (seqBRCA2-Rev + exon2-For: CGGCGGCGTTCAGAATCAGGCTC).

POLQ knockout cells were generated as well in U2OS cells. Cas9 was introduced into U2OS cells by lentiviral infection using the lentiCas9-Blast plasmid (Addgene #52962), and stable Cas9-expressing U2OS cells (U2OS-Cas9) were obtained after blasticidin selection. SgRNA oligos designed to target the genomic sequence GATTCGTTCTCGGGAAGCGG of *POLQ* (exon 1) were annealed and inserted into LentiGuide-Puro plasmid (a gift from Feng Zhang, Addgene #52963). After lentivirus infection, U2OS-Cas9 cells were selected by

puromycin for 3 days, and the survived cells were trypsinized and seeded sparsely to form single-cell colonies. Colonies were picked and expanded, and genomic DNA from individual clones was isolated by QIAamp DNA Mini Kit (Qiagen). PCR was performed to amplify the gRNA-targeted region (216 bp), using the following primers: Forward, GGAGGACGCTGGGACTGTGGC; Reverse, CTGCAGCTGCGGCCTTCAGGC. PCR products were cleaned by PCR purification kit (Qiagen) and submitted for Next-Gen Sequencing (Amplicon sequencing provided by Genewiz). The sequencing reads were mapped to the human genome at *POLQ* locus and the results were visualized by Integrative Genomics Viewer (IGV, Broad Institute). Clones with homologous deletion of *POLQ* gene were confirmed by Western blot analysis. Western blots were collected using Odyssey Infrared Imagers (Li-Cor), and analyzed using Image Studio Lite.

Cloning, PiggyBac constructions and cell line generation

Wild type (WT) full length *POLQ* cDNA was assembled by PCR with a FLAG-P2A-BLAST cassette and subsequently cloned by Gibson assembly (New England BioLabs, #E2611L) in the PiggyBac PBCAG-eGFP vector (Addgene #40973) using BsrGI and SbfI sites to obtain the PiggyBac-eGFP-POLQ-FLAG-P2A-BLAST vector (referred here as GFP-Polθ WT). Point mutations were introduced using PCR mutagenesis and Gibson assembly in active sites as follow: Helicase (K121A, DE-216/7-AA), polymerase (DE-2540/1-AA), helicase/polymerase (K121A, DE-216/7-AA, DE-2540/1-AA). RPE1b POLQ$^{-/-}$ cells were complemented with GFP-Polθ WT and mutant constructs. Cells were plated in a 6-well plate, transfected the day after with 1 μg of PiggyBac vector and 0.5 μg of PiggyBac transposase (System Biosciences, #PB210PA-1) using Lipofectamine LTX with Plus Reagent (Thermo Fisher) and selected with Blasticidin (21 μg/ml) for 10 days. Vectors expression was confirmed by Western Blot.

Laser micro-irradiation

RPE1b POLQ$^{-/-}$ cells expressing eGFP-POLθ constructs were plated in a 35 mm μ-Dish with glass bottom (Ibidi, #81158). The day after, DMSO (0.1%) or Novobiocin (NVB, 100 μM) were added to the cells for 16 hours. Media was replaced by fresh one (with DMSO or NVB) 2 hours prior the irradiation. Micro-irradiations were performed with a two photons laser (800 nm, 20% power) on an inverted Laser Scanning Confocal Microscope equipped with Spectral Detection and Multi-photon Laser (LSM880NLO/Mai Tai Laser - Zeiss/ Spectra Physics) with Airyscan module. Images were analyzed using “Plot Z-Axis Profile” macro on Fiji (version 2.1.0/1.53c). RPE1b POLQ$^{-/-}$ cells expressing PBCAG-eGFP vector were used as a control.

Mouse Xenograft and PDX studies

All animal experiments were conducted in accordance with Institutional Animal Care and Use Committee-approved protocols at Beth Israel Deaconess Medical Center and Dana-Farber Cancer Institute. For PDX studies, tumor ascites were collected from patients with suspected or established ovarian cancer at the Brigham and Women’s Hospital or the Dana-Farber Cancer Institute (DFCI) under IRB-approved protocols conducted in accordance with the Declaration of Helsinki and the Belmont Report. Written informed consent was obtained from patients when required.

TOV21G xenograft study: Female NU(NCr)-*Foxn1*^{nu} athymic nude mice were purchased from Charles River for TOV21G xenograft experiments. 5×10^5 of TOV21G+EV or TOV21G+FANCF cells in PBS were mixed with equal volume of Matrigel (Corning) and injected subcutaneously to the flank of the mice. The mice were then randomly assigned to 4 treatment groups: (1) TOV21G+EV:PBS, (2) TOV21G+EV:NVB, (3) TOV21G +FANCF:PBS, and (4) TOV21G+FANCF:NVB. 4 days after tumor cell implantation, the mice were treated with NVB (100 mg/kg) or PBS twice a day via intraperitoneal injection (IP injection) for 4 weeks. Tumors were measured every 2 to 3 days using an electronic caliper, and tumor volumes were calculated by using the formula L×W×W/2.

GEMM: Pieces from breast tumors generated in K14-*Cre-Brca1*$^{f/f}$*Trp53*$^{f/f}$ female mice were transplanted into the mammary fat pad of FVB/129P2 recipient females that were at least 6 weeks old. FVB/129P2 recipients were generated by breeding FVB females (Jackson Laboratories) and 129P2 males (Envigo) and using the first-generation litters for experimentation. When tumors reached approximately 150 mm^3 in volume mice were randomized into treatment groups (vehicle and NVB). Treatments continued until tumors reached 20 mm in any direction, at which point mice were euthanized. NVB was prepared fresh from powder in PBS each time before IP injection and administered at 100 mg/kg twice a day for 35 days. Tumors were measured every 3 to 4 days using an electronic caliper, and tumor volumes were calculated by using the formula L×W×W/2.

PDX studies: PDX models were established, luciferized and propagated at the DFCI and have been described previously [57]. Approximately 2–10 $\times 10^6$ luciferized PDX cells derived from mouse ascites were injected intraperitoneally into 8-week old female NSG mice. Tumor burden was measured by bioluminescence imaging (BLI) using a Xenogen IVIS-200 system (Xenogen). Mice were grouped according to their BLI signal from tumors so that each group would have similar initial average BLI. NVB was diluted in saline and administered via IP injection at 75 mg/kg twice daily for 4 weeks. Olaparib (ChemExpress) was formulated in PBS containing 10% DMSO and 10% (wt/vol) 2-hydroxypropyl- β-cyclodextrin (Sigma-Aldrich) and administered orally at 50 mg/kg daily for 4 weeks.

Quantitative RT-PCR

Total RNA was extracted using the RNeasy Mini kit (Qiagen), and cDNA was generated using the SuperScript™ III First-Strand Synthesis kit (Thermo Fisher). The PowerUp SYBR Green Master Mix (Thermo Fisher) reagent was used to run quantitative PCR on a QuantStudio 7 Flex Real-Time PCR System (Applied Biosystems). Two set of POLQ primers were used which gave same POLQ mRNA measurements. POLQ primer set 1 (forward: 5-TATCTGCTGGAACTTTTGCTGA-3; reverse: 5-CTCACACCATTTCTTTGATGGA-3); POLQ primer set 2 (forward: 5-CTACAAGTGAAGGGAGATGAGG-3; reverse: 5-TCAGAGGGTTTCACCAATCC-3). Internal control primers are beta-Actin (forward: 5-CACCATTGGCAATGAGCGGTTC-3; reverse: 5-AGGTCTTTGCGGATGTCCACGT-3) or GAPDH (forward: 5-GTCTCCTCTGACTTCAACAGCG-3; reverse: 5-ACCACCCTGTTGCTGTAGCCAA-3).

Immunohistochemistry (IHC)

NSG mice bearing DF-59 and DF-83 tumors were dosed as in the efficacy study, with 75 mg/kg NVB twice a day and 50 mg/kg Olaparib daily. 4 hours after last dose (52 hours after first dose), tumor cells were isolated from the peritoneum of the mice, cleaned, washed with PBS and fixed in 10% normal buffered formalin for 10 min at RT. Next, the tumor cells were washed with PBS 3X and embedded in Histogel (Richard Alen Scientific). Histogel cores were processed using standard histology methods and embedded in paraffin. RAD51 staining was performed on paraffin sections (4 μm) using a previously standardized protocol (https://doi.org/10.1158/1538–7445.AM2017–2796). Images of stained slides were acquired on an Olympus BX41 microscope equipped with a digital camera at 40X magnification. The percentage of RAD51-foci positive cells fields was estimated.

Molecular Docking

We used the AMP-PNP-Mg^{2+} bound POLθ-HD (PDB ID-5AGA) structure for our docking studies as it has the best resolution (2.9 Å) among the reported structures in the protein data bank (PDB) [30]. For the docking studies, the protein structure is prepared using Protein Preparation Wizard from the Schrödinger suite. The AMP-PNP-Mg^{2+} was stripped from the structure as well. Using the minimized structure, a 25 Å grid created around the Asn451 residue given its close proximity to the ADP/AMP-PNP binding site in the helicase domain for the search of a potential binding site for Novobiocin. The LigPrep Wizard from the Schrödinger suite is used to prepare novobiocin ligand in different protonated states for the docking. All minimizations in the Protein Prep and LigPrep wizards are performed with OPLS3 force field [58]. Glide Extra Precision docking module of the Schrödinger workflow is used for producing novobiocin and POLθ-HD complex structure with the best scoring poses [59]. For all the generated poses, binding free energy MM-GBSA calculations were performed using the Prime module and the best model selected based on the resulting protein-ligand complex with a lowest MM-GBSA binding free energy value [60].

Statistics and Reproducibility

No statistical methods were used to predetermine sample sizes. The experiments were not randomized except for mouse studies, where mice were randomized based on their initial tumor sizes to achieve an approximately equal mean. No data were excluded from the analyses. The person who performed the mouse xenograft studies was blinded to the identities of the tumor cells. The person who performed the PDX studies was blinded to the genotypes of the tumors being studied. For other studies, no specific blinding method was used. The statistical analyses performed were specified in the figure legends. Statistical analyses were performed in Prism version 8 (GraphPad). Error bars represent ±SD or ±SEM as described in figure legends, and p values are indicated by *$p < 0.05$, **$p < 0.01$, ***$p < 0.001$, ****$p < 0.0001$, unless values are given.

Reporting Summary.—Further information is available in the Nature Research Reporting Summary linked to this article.

Data Availability

All related data have been presented in this manuscript. Source data for each Figure and Extended Data Figure have been provided as Source Data files. Complete results of small molecule screen and lists of top hits have been provided in Supplementary Tables 1–4.

Code Availability

No code was generated or used for this study.

Extended Data

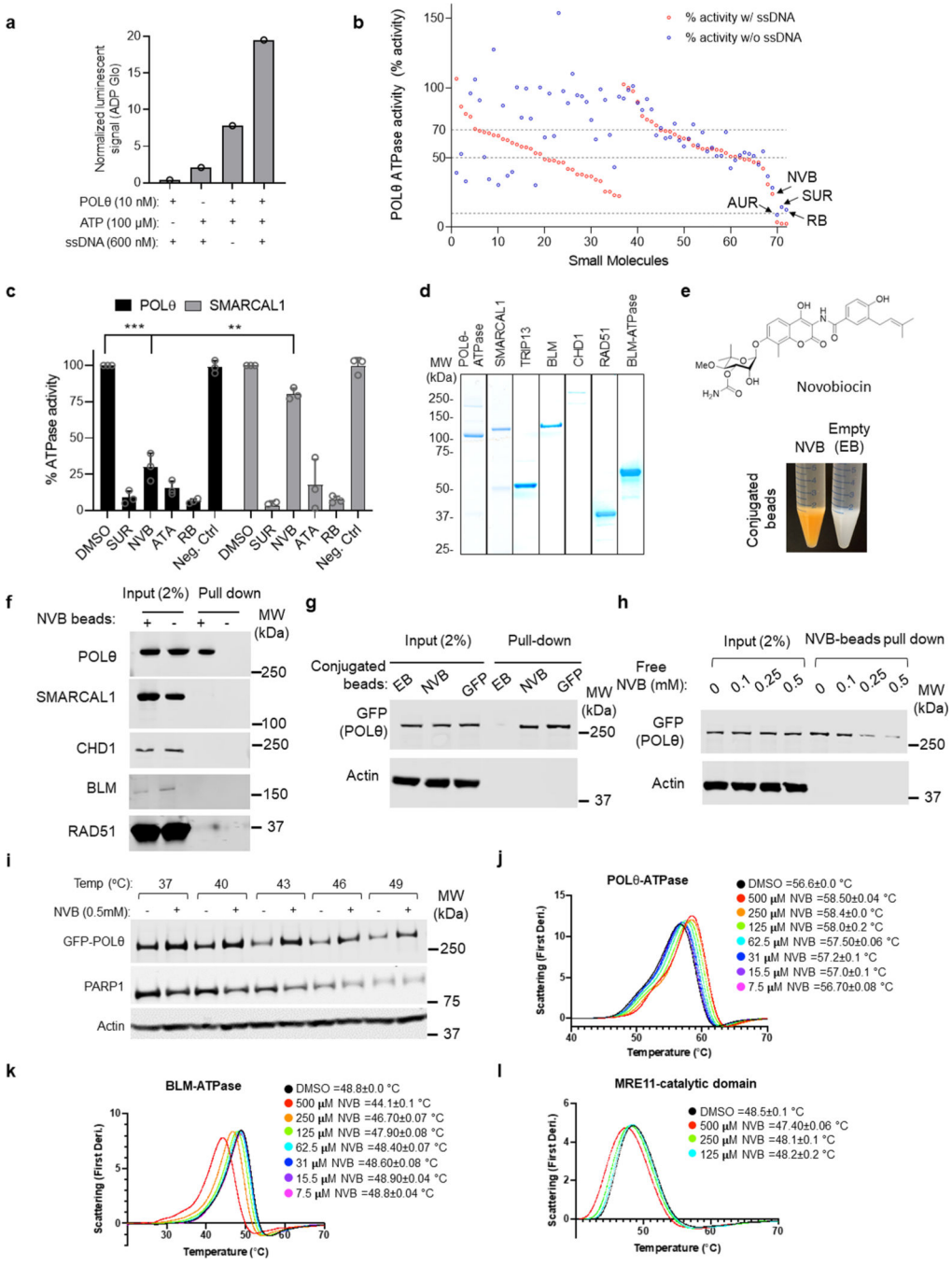

Extended Data Fig. 1. Characterization of POLθ inhibitors obtained from the small-molecule screen, with biochemical assays and cell-based assays.Characterization of POLθ inhibitors obtained from the small-molecule screen, with biochemical assays and cell-based assays.

a, ADP-Glo assay for quantification of POLθ ATPase activity in various experimental conditions. N = 1 experiment. **b**, A secondary screen using the 72 initial hits in reducing POLθ ATPase activity (below 70 %, *z*-score < −4). The screen was done in the presence and absence of ssDNA. The four most promising hits advancing for further analysis are labeled

(see Table S4 for analysis). Aurintricarboxylic acid (ATA), Reactive Blue 2 (RB), Suramin (SUR), and Novobiocin (NVB). Data shown are mean of n=2 independent experiments. **c**, Quantification of POLθ and SMARCAL1 ATPase activity with indicated small molecules. The negative control is an inert small molecule (Vandetanib). Data shown are mean ± SD, n=3 independent experiments. Statistics were performed using two tailed *t*-test with Welch's correction. ***$p < 0.001$, **$p < 0.01$. **d.** Coomassie blue stained gels showing purified ATPase that were used in this study. **e**, Conjugation of NVB to epoxy-activated Sepharose-6B (Sigma). NVB conjugated beads showed light yellow color. The structure of NVB is shown. **f**, Pulldown experiments with NVB-conjugated beads and purified POLθ, SMARCAL1, CHD1, BLM, and RAD51. POLθ, SMARCAL1, CHD1, and BLM were detected by Western blot using anti-Flag antibody (Sigma #F1804) in this assay. RAD51 was detected by anti-RAD51 antibody (SantaCruz #398587). **g**, Pulldown experiments with NVB-conjugated beads and cell lysate from HEK293T cells expressing GFP-tagged full-length POLθ. Cell lysates were incubated with empty beads (EB), NVB-beads (NVB) or anti-GFP-beads (GFP) to assay for direct POLθ binding. GFP-POLθ bound to beads and input of each group were subjected to Western blot analysis, using an anti-GFP antibody. **h**, Competition assay between NVB-conjugated beads and free NVB when incubated with GFP-tagged full-length POLθ extracted from HEK293T cells. **i**, Thermal shift assay using GFP-POLQθ expressing HEK293T cell lysate incubated with NVB at the indicated temperatures. Supernatants after heat treatment were subjected to Western blot using anti-GFP and anti-Actin antibodies. **J-l**, Titration of indicated NVB (or DMSO) concentration with POLθ (**j**), BLM (**k**), or MRE11 (**l**) in the thermal shift assay to measure the effect of NVB on the protein stability. Average first derivative of the scattering profile is shown. Scattering peak max values are shown as mean ± SD, from n=3 independent experiments.

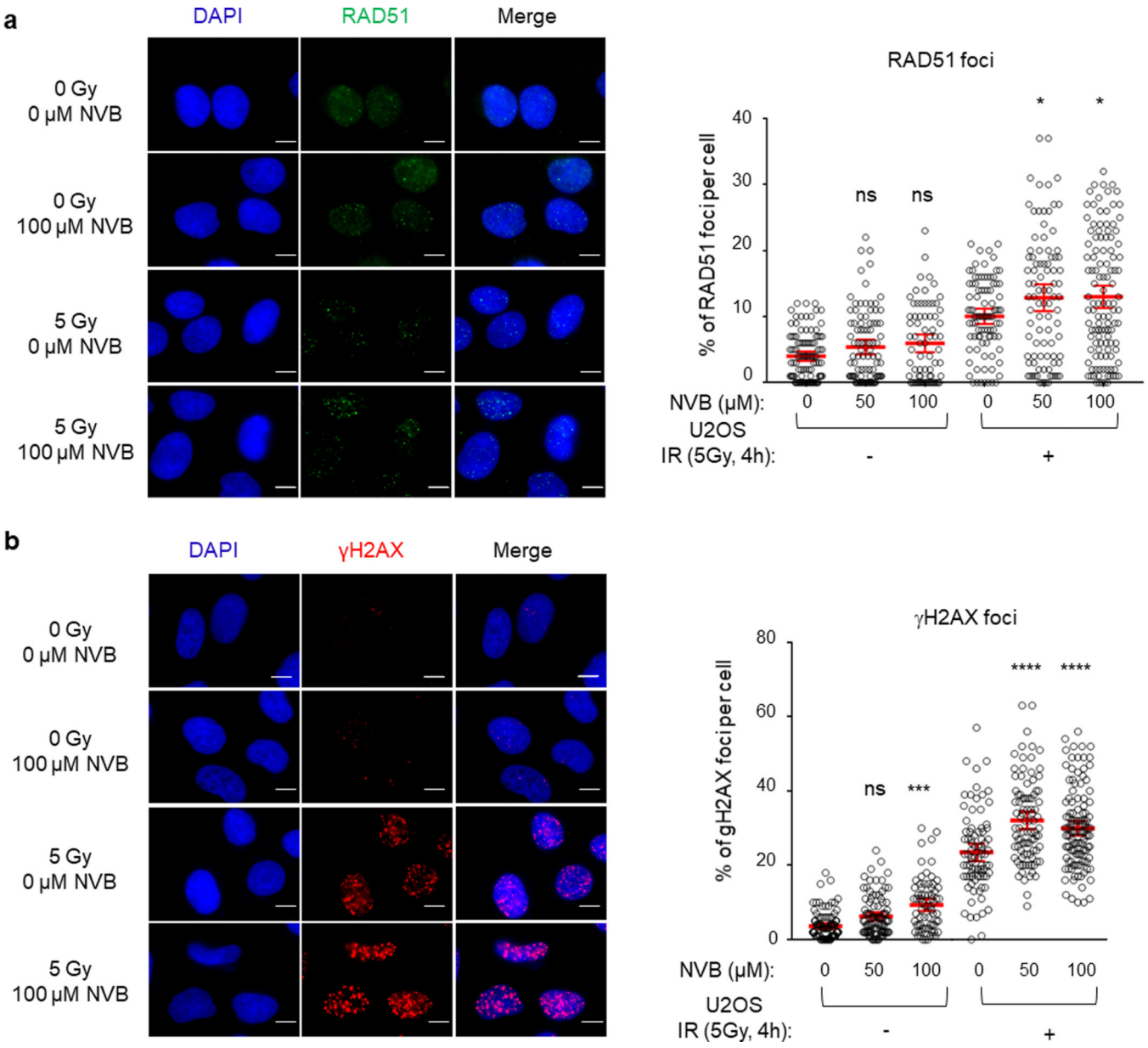

Extended Data Fig. 2. Novobiocin phenocopies POLθ depletion in human cells. Novobiocin phenocopies POLθ depletion in human cells.

a, Images and quantification of RAD51 foci in U2OS cells under increasing concentrations of NVB with or without gamma-irradiation (IR). **b**, Images and quantification of γH2AX foci in U2OS cells under increasing concentrations of NVB with or without IR. Data in (**a**) and (**b**) were pooled from two independent experiments. Each dot represents foci numbers

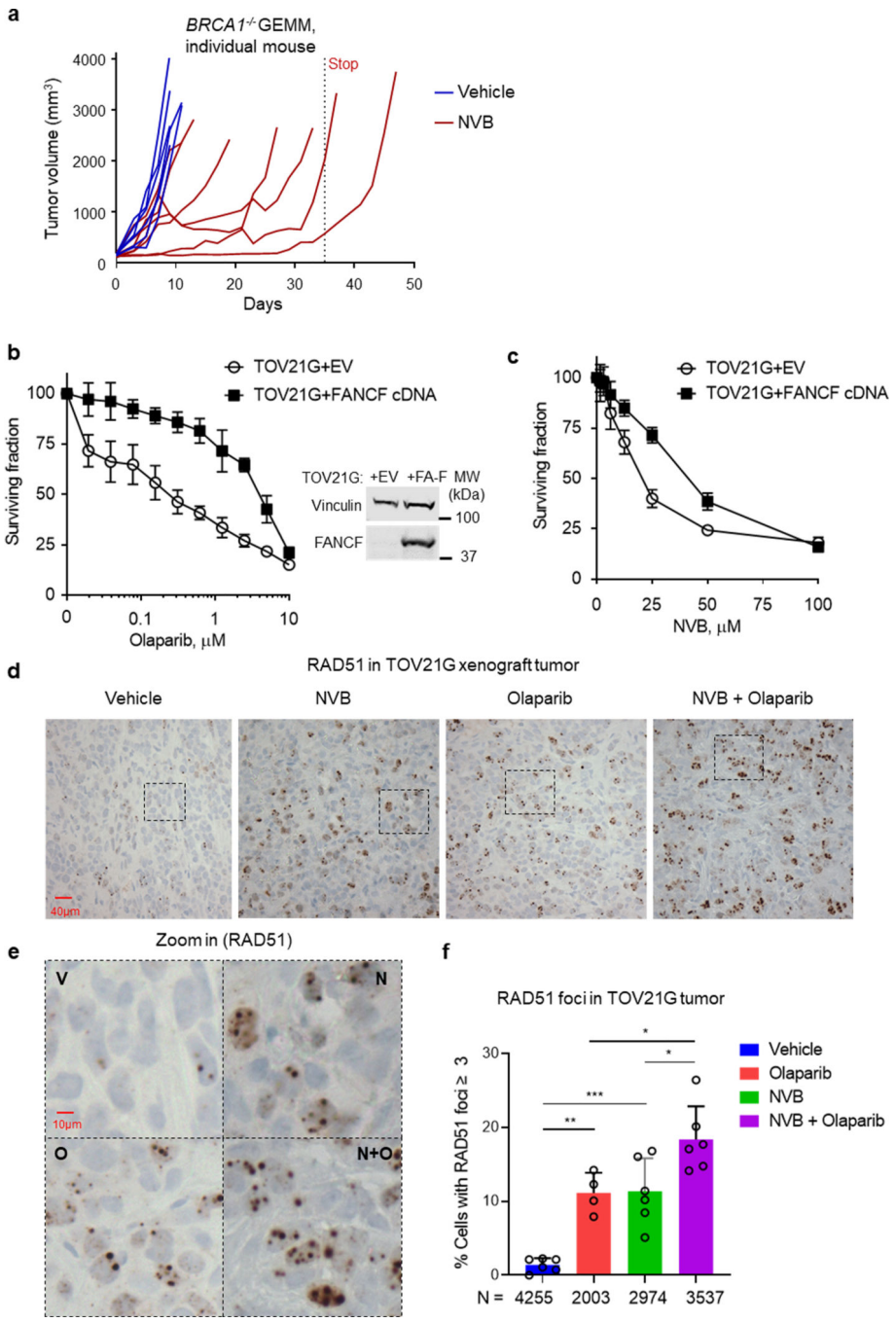

Extended Data Fig. 3. Efficacy of NVB in *BRCA1*$^{-/-}$ GEMM and RAD51 PD study in TOV21G xenograft models. Efficacy of NVB in *BRCA1*$^{-/-}$ GEMM and RAD51 PD study in TOV21G xenograft models.

a, NVB efficacy in the GEMM model (*Tp53*$^{-/-}$*Brca1*$^{-/-}$ TNBC). Response of each tumor in each individual mouse is shown. Tumor chunks from GEMM mice were implanted in syngeneic FVB/129P2 mice, which were treated with PBS or 100 mg/kg NVB twice a day via IP for 5 weeks. **b**, Olaparib sensitivity of TOV21G (+ EV) or FANCF-complemented TOV21G (+ FANCF cDNA). **c,** Novobiocin sensitivity of TOV21G (+ EV) or FANCF-complemented TOV21G (+ FANCF cDNA). Mean ± SD of n=6 biologically independent

samples are shown in **b and c**. **d-f**, Immunohistochemical (IHC) study of the pharmacodynamic biomarker RAD51 after NVB and/or olaparib treatment in TOV21G tumors. **d,** Representative images of RAD51 IHC staining in xenografted TOV21G tumor cells. Tumor bearing NU(NCr)-Foxn1nu mice were treated with indicated drugs for 18 days before tumors were taken. FFPE tissue sections of the tumors were stained using an anti-RAD51 antibody and representative images (40X) are shown. **e**, Zoom-in of the IHC images in **(d)** to show RAD51 foci in detail. **f**, Quantification of RAD51 foci positive cells in TOV21G tumors. Cells with three or more RAD51 foci were counted as positive cells. Tumor samples from each group were processed and analyzed, and Mean±SD are shown, n=4 for Olaparib and n=6 for other groups. The total number of cells counted were shown in the graph (N). Statistical analysis was performed using one-way ANOVA in Prism, *, $p < 0.05$; **, $p < 0.01$; ***, $p < 0.001$.

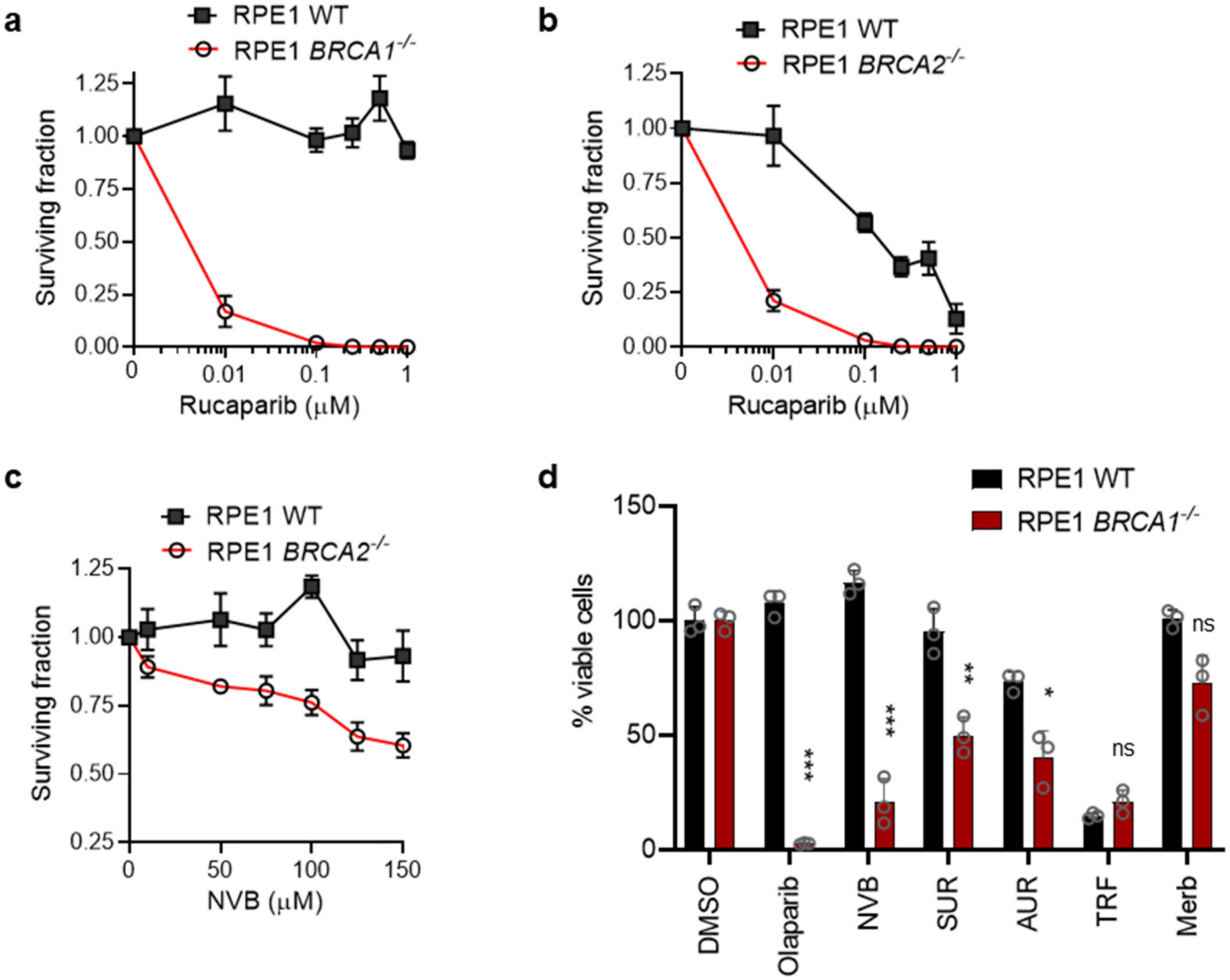

Extended Data Fig. 4. Effects of novobiocin in *BRCA1*$^{-/-}$ and *BRCA2*$^{-/-}$ cells. Effects of novobiocin in *BRCA1*$^{-/-}$ and *BRCA2*$^{-/-}$ cells.

a, Clonogenic survival of *BRCA1*$^{-/-}$ and WT RPE1 cells under increasing concentrations of the PARPi rucaparib. **b**, Clonogenic survival of *BRCA2*$^{-/-}$ and WT RPE1 cells under increasing concentrations of PARPi rucaparib. **c**, Clonogenic survival of *BRCA2*$^{-/-}$ and WT RPE1 cells under increasing concentrations of POLθ inhibitor. The survival fraction in **a-c** is normalized to the untreated samples. Data shown are Mean ± SEM, n = 3 independent experiments. **d**, Cell viability assay (CellTiter-Glo) in *BRCA1*$^{-/-}$ and WT RPE1 cells treated with indicated POLθ inhibitors (50 μM) or with the PARPi Olaparib as control. Cells were treated twice on days 1 and 4 and cell viability was measured on day 7. Data were mean ± SD, n = 3 biological replicates. Statistics analyses were two tailed *t*-test. *, $p < 0.05$; **, $p < 0.01$; ***, $p < 0.001$, ns, not significant ($p > 0.05$).

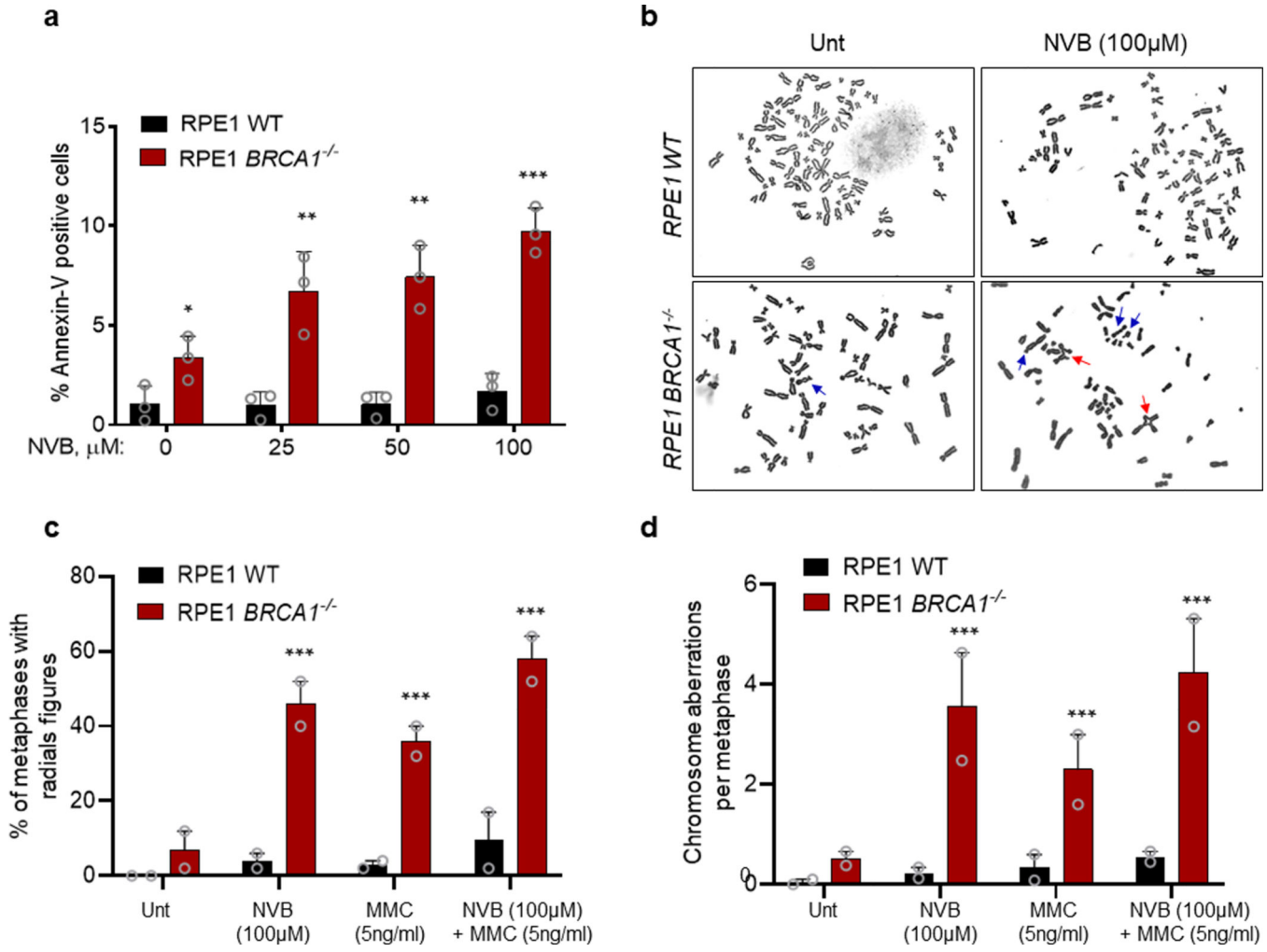

Extended Data Fig. 5. NVB induces apoptosis and chromosome aberrations in *RPE1 BRCA1*$^{-/-}$.
NVB induces apoptosis and chromosome aberrations in *RPE1 BRCA1*$^{-/-}$.

a, Quantification of apoptosis in *BRCA1*$^{-/-}$ and WT RPE1 cells under increasing concentrations of NVB. Mean ± SD, n = 3 independent experiments. **b,** Representative images of chromosomal aberrations (blue arrows) including radial figures (red arrows) in RPE1 (WT or *BRCA1*$^{-/-}$) cells treated with NVB. **c-d**, Quantification of radial figures (**c**) and total chromosome aberration (**d**) in *BRCA1*$^{-/-}$ and WT RPE1 cells treated with NVB

alone or in combination with mitomycin C (MMC). Data in **c-d** are mean ± SD of n = 3 independent experiments. Statistical significance was determined by one-way ANOVA multiple comparisons using uncorrected Fisher's LSD test. ***, $p < 0.001$.

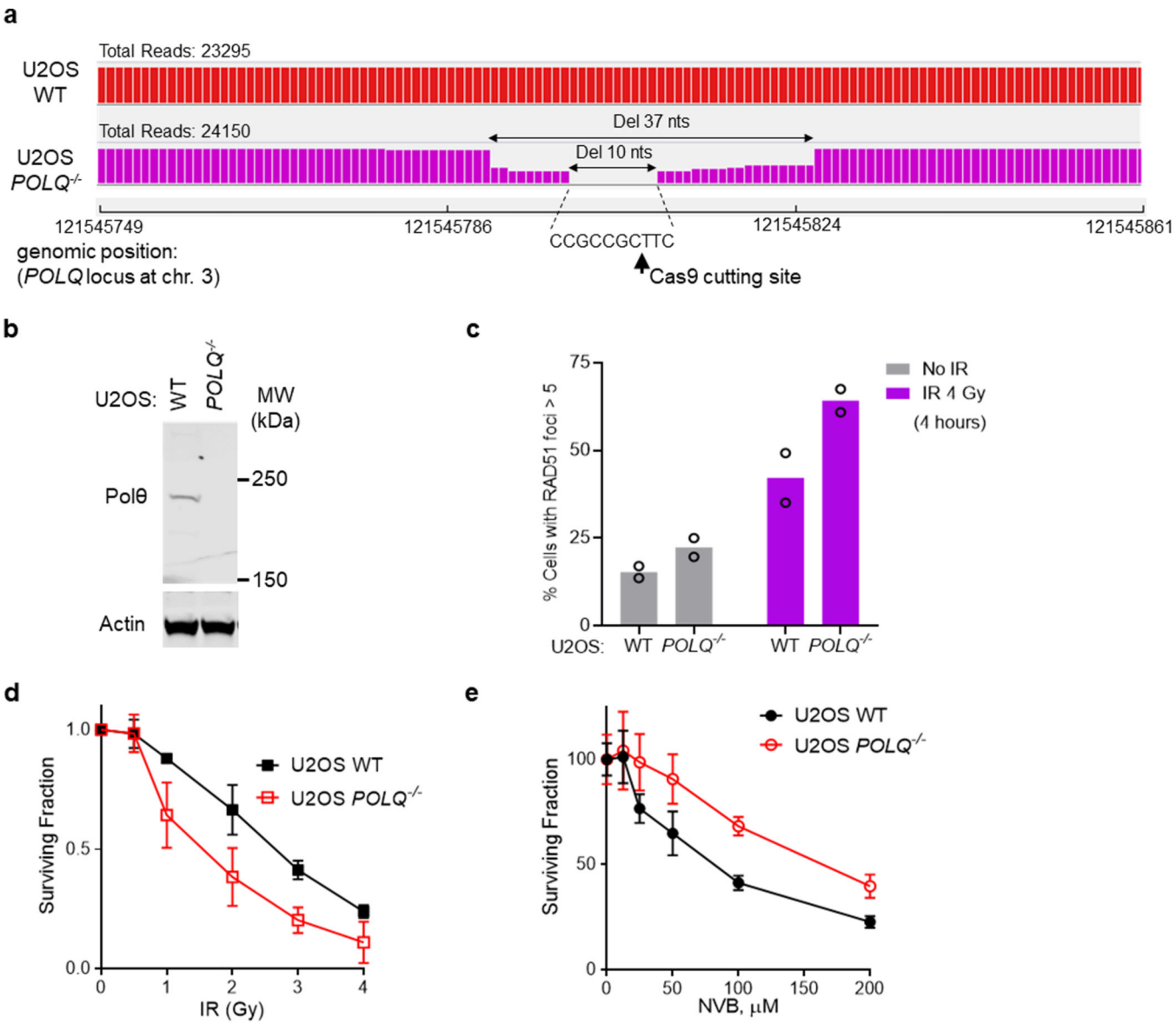

Extended Data Fig. 6. *POLQ*$^{-/-}$ U2OS cells were resistant to NVB. *POLQ*$^{-/-}$ U2OS cells were resistant to NVB.

a-d, Verification of the U2OS-*POLQ*$^{-/-}$ cell line. **a**, Mapping the genetic alteration (deletions) in the U2OS *POLQ* knockout clone generated by CRISPR-Cas9. The targeted region was sequenced by Next Gen sequencing (number of reads are shown), and the deletions were mapped to *POLQ* locus of human genome on chromosome 3. **b**, A Western blot showing POLθ protein expression in WT and *POLQ*$^{-/-}$ U2OS cells. **c**, RAD51 foci assay in WT or *POLQ*$^{-/-}$ U2OS cells before and after (4 h) of 4 Gy IR. Mean of n=2 independent experiments is shown. **d**, IR sensitivity of WT and *POLQ*$^{-/-}$ U2OS cells in

clonogenic assays. Mean ± SD of n=3 independent experiments are shown. **e**, NVB sensitivity of WT and *POLQ*$^{-/-}$ U2OS cells in clonogenic assays. Mean ± SD of n=6 biologically independent samples are shown.

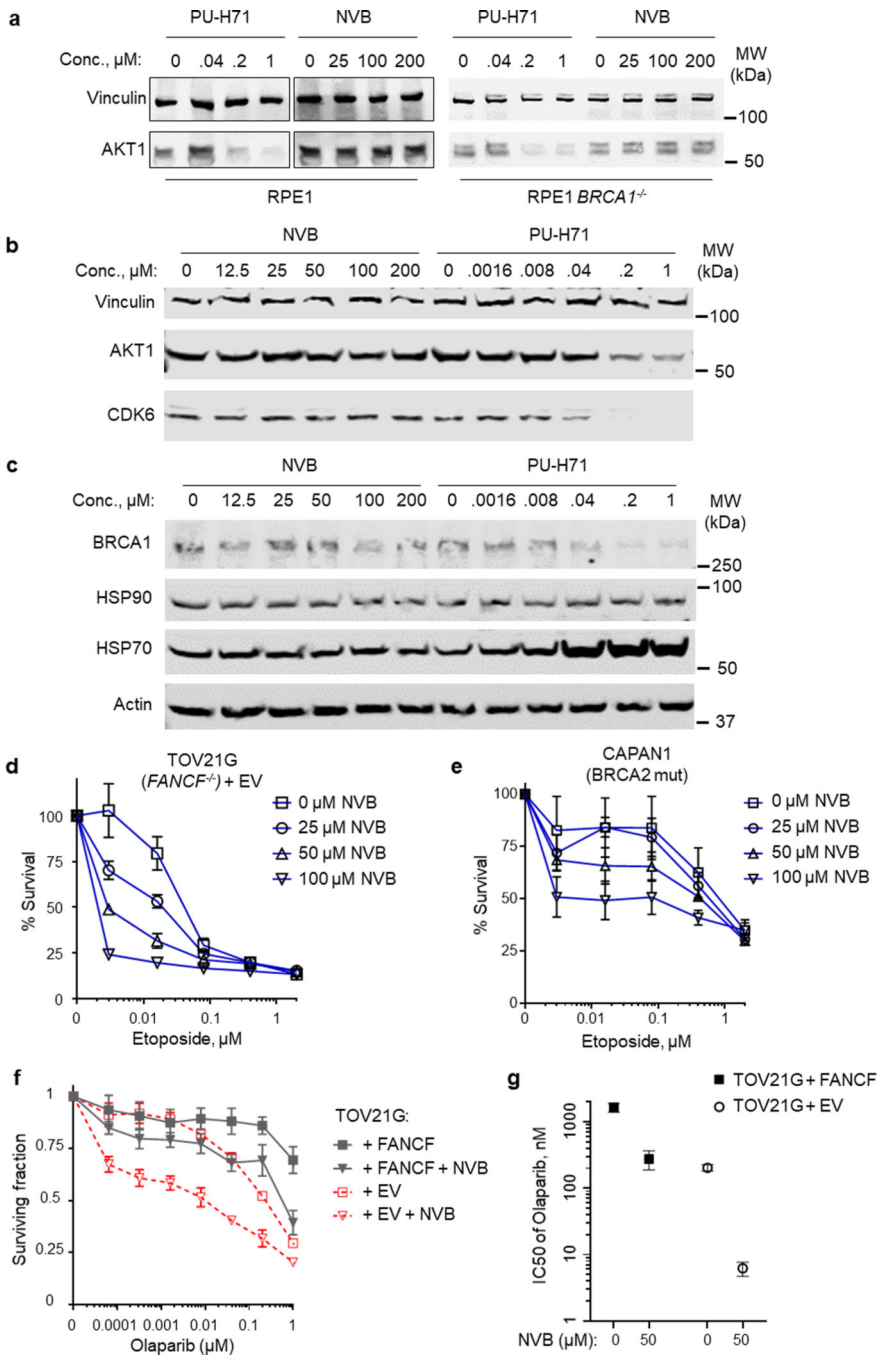

Extended Data Fig. 7. NVB inhibits POLθ but not HSP90 or TOP2 in human cells. NVB inhibits POLθ but not HSP90 or TOP2 in human cells.

a, HSP90 client degradation assay in RPE1 and RPE1-*BRCA1*$^{-/-}$ cells. Cells were treated with a potent HSP90 inhibitor PU-H71 or NVB for 48 hours, and then cells were collected for Western blot analysis of the HSP90 client AKT1. **b-c**, HSP90 client degradation assay in

MCF7 cells. Cells were treated with the potent HSP90 inhibitor PU-H71 or NVB for 24 hours, and then cells were collected for Western blot analysis of the HSP90 client proteins AKT1, CDK6 (**b**) and BRCA1 (**c**). Levels of HSP90 and HSP70 were also analyzed after NVB or PU-H71 treatment (**c**). **d-e**, Combination effect of etoposide and novobiocin in killing TOV21G cells (**d**) and CAPAN1 cells (**e**), showing their non-epistatic effects. Mean ± SD of n=3 independent experiments are shown. **f**, CellTiter-Glo cell viability assay of empty vector (EV) and FANCF-complemented TOV21G cells, in the presence of olaparib, novobiocin or both. Mean ± SD, n = 4 biological replicates are shown. **g**, IC_{50} values of olaparib in TOV21G cells with or without NVB, derived from data in **f**. Mean ± SD of IC_{50} were shown, from n = 4 biological replicates.

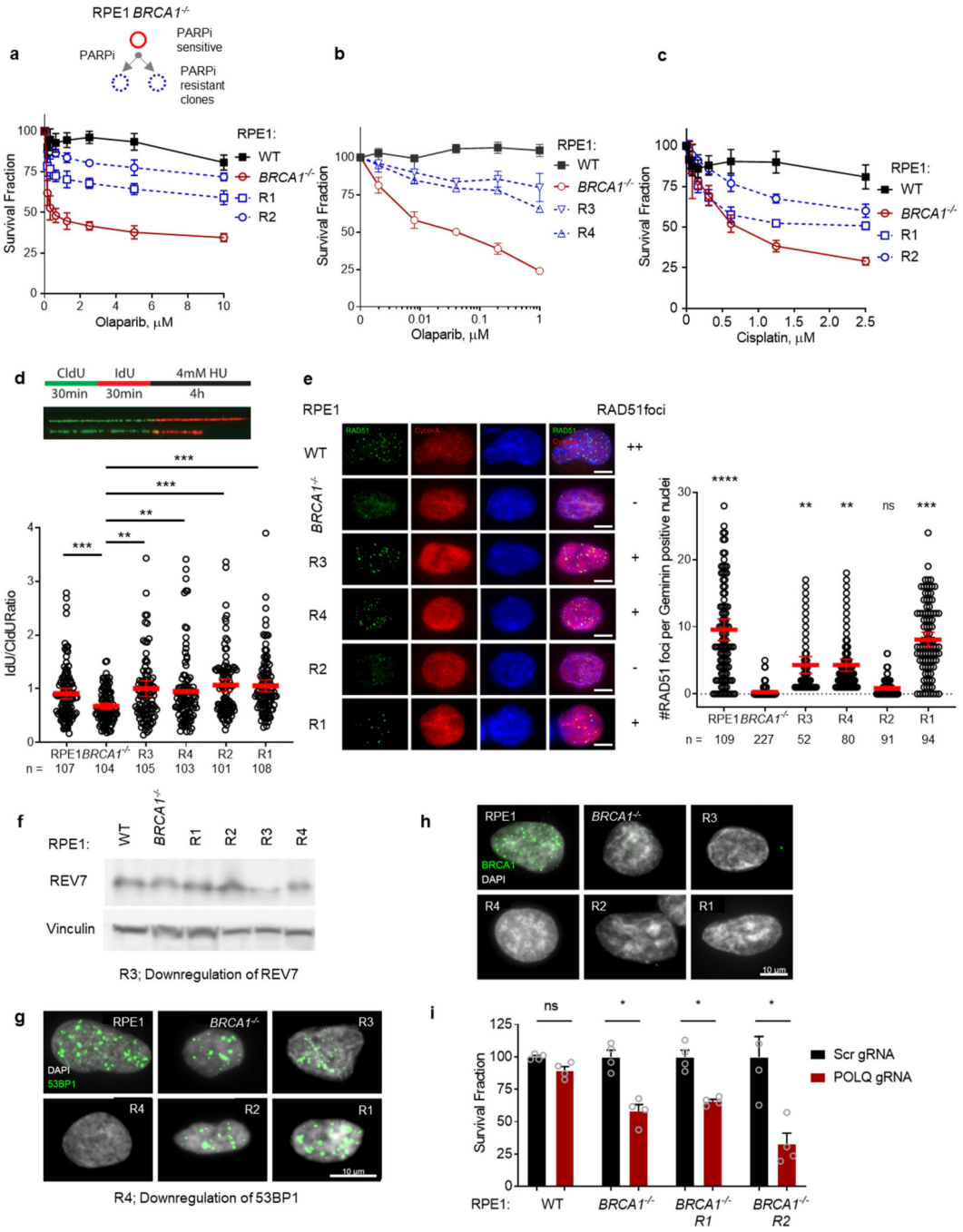

Extended Data Fig. 8. Characterization of PARP inhibitor resistant clones derived from RPE1-*BRCA1*$^{-/-}$.Characterization of PARP inhibitor resistant clones derived from RPE1-*BRCA1*$^{-/-}$.

a-c, Olaparib (**a-b**) and cisplatin (**c**) sensitivity of WT and *BRCA1*$^{-/-}$ RPE1 cells and the PARPi resistant clones of *BRCA1*$^{-/-}$ RPE1. Mean ± SD of biological replicates are shown, with n=8 in **A**, n=3 in **B**, and n=8 in **C**. **d**. DNA fiber assay to measure the replication fork stability of the PARPi resistant clones. Mean±95%CI are shown from 3independent experiments are shown, with n = number of fibers scored labeled. **e**. RAD51 foci analysis in WT and *BRCA1*$^{-/-}$ RPE1 cells and the PARPi resistant clones after irradiation (5Gy), to

determine restoration of RAD51 foci in R clones. RAD51 was stained 4 hours after IR. Scale bar = 10 μm. **f**, A Western blot of WT and *BRCA1*$^{-/-}$ RPE cells and the PARPi resistant clones using a REV7 antibody. **g**, Immunofluorescence staining of 53BP1 in WT and *BRCA1*$^{-/-}$ RPE1 cells and the PARPi resistant clones after irradiation. Clone R4 showed much reduced 53BP1 foci after IR. **h,** Immunofluorescence staining of BRCA1 in WT and *BRCA1*$^{-/-}$ RPE1 cells and the PARPi resistant clones after irradiation. No BRCA1 foci was observed except in WT RPE1 cells. **i**, CellTiter-Glo assay to determine survival of PARPi-resistant and parental *BRCA1*$^{-/-}$ RPE1 cells upon CRISPR knockout of the *POLQ* gene. Data are mean ± SEM, with n = 4 biological replicates. Statistical analysis was *t*-test, *, $p < 0.05$; ns, not significant.

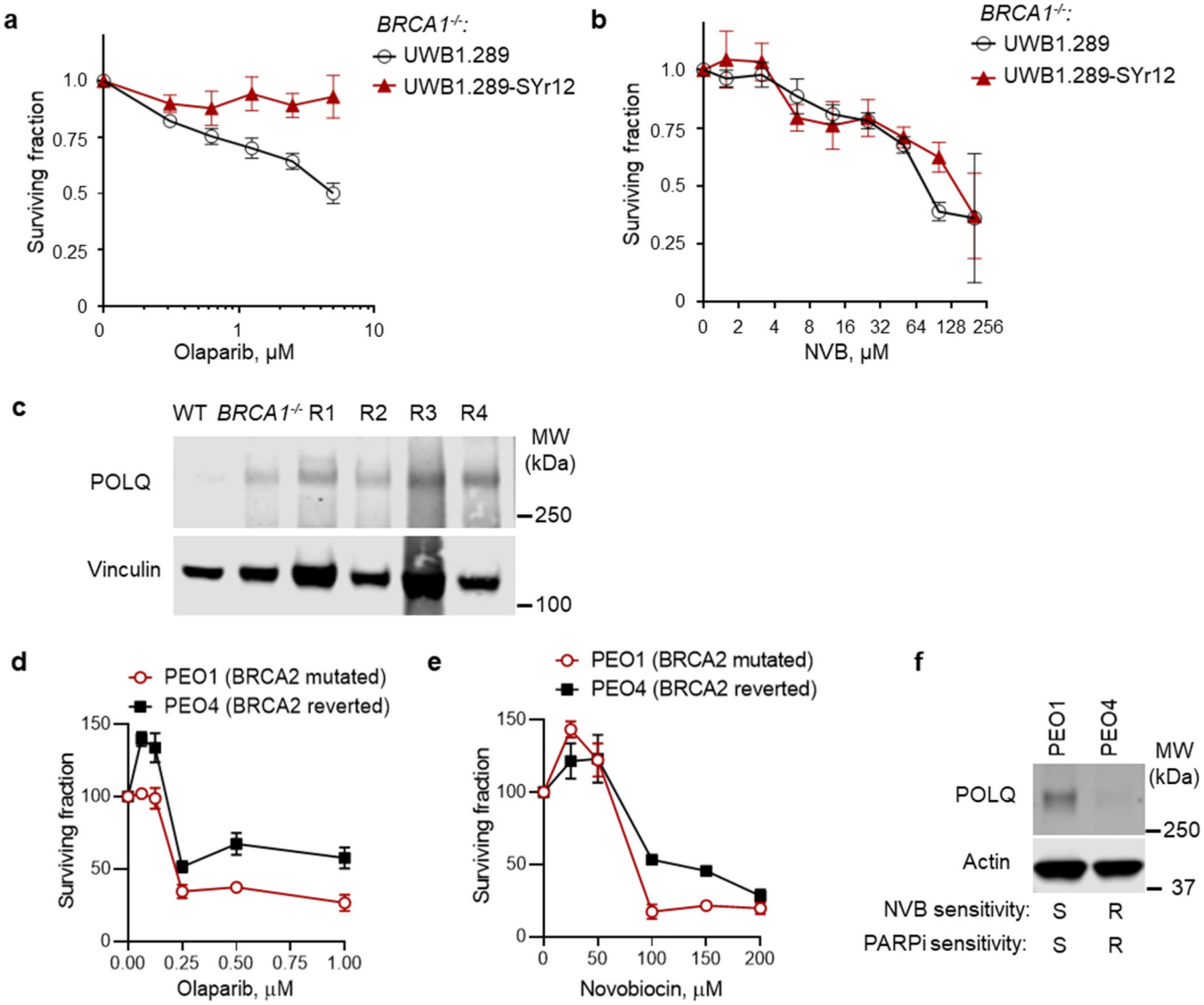

Extended Data Fig. 9. PARPi resistant MDA-MB-436 and UWB1.289 cells are sensitive to NVB, and NVB has synergy with PARPi in TOV21G cells. PARPi resistant MDA-MB-436 and UWB1.289 cells are sensitive to NVB, and NVB has synergy with PARPi in TOV21G cells.

a-b, Olaparib (**a**) and NVB (**b**) sensitivity of UWB1.289 and a PARPi resistant UWB1.289 clone (UWB1.289-YSR12) in CellTiter-Glo assays. Data shown are mean ± SD, n = 4 biological replicates. **c**. Western blot analysis of POLQ expression levels in in WT and *BRCA1*$^{-/-}$ RPE1 cells and the PARPi resistant *BRCA1*$^{-/-}$ clones. **d.** Olaparib sensitivity of PEO1 (BRCA2 mutated) and PEO4 cells (BRCA2 restored). **e**. NVB sensitivity of PEO1 and PEO4 cells. Data shown in **d** and **e** are Mean ± SD, n= 3 biological replicates. **f**. A Western blot shows POLQ expression in BRCA2-decient cells lines (PEO1) and their counterparts with BRCA2 reverted to wild type (PEO4).

Supplementary Material

Refer to Web version on PubMed Central for supplementary material.

ACKNOWLEDGEMENTS

We thank the ICCB-Longwood Screening Facility at Harvard Medical School, for their help in small-molecule screening. We thank Prafulla Gokhale and Qing Zeng at the Belfer Center for Applied Cancer Science, as well as Chunyu Yang and Kalindi Parmar at the Center for DNA Damage and Repair, for their help in mouse studies. We thank Connor Clairmont for providing RPE *BRCA1*$^{-/-}$ cells and purified TRIP13 protein and Lisa Moreau for her help in chromosome aberration assays. We thank Huy Nguyen and Sandor Spisak for genomic analysis of the *POLQ* knockout clones. We thank Dr. Chi-Lin Tsai at MD Anderson Cancer Center for providing the BLM-ATPase expression vector. We thank Dr. Jeremy Stark for providing DR-GFP and EJ-2 repair substrates, and Dr. Gaëlle Legube for providing the DIvA cells for DSB end resection assays.

This research was supported by a Stand Up To Cancer (SU2C)-Ovarian Cancer Research Fund Alliance-National Ovarian Cancer Coalition Dream Team Translational Research Grant (SU2C-AACR-DT16-15) to A.D.D. SU2C is a program of the Entertainment Industry Foundation. Research grants are administered by the American Association for Cancer Research, the scientific partner of SU2C. This work was also supported by the NIH (grants R37HL052725, P01HL048546, P50CA168504), the US Department of Defense (grants BM110181 and BC151331P1), as well as grants from the Breast Cancer Research Foundation and the Fanconi Anemia Research Fund to A.D.D. This work was also supported by the Richard and Susan Smith Family Foundation, the Breast Cancer Research Foundation (BCRF-20-033), and the Basser Initiative at Gray Foundation (167858/167856) to A.D.D. This work was also supported by the ERC starting grant (N° 714162) and the Ville de Paris Emergences Program grant (N° DAE 137) to R.C. This work was also supported by Ann Schreiber Mentored Investigator Award from Ovarian Cancer Research Fund Alliance (457527), Joint Center for Radiation Therapy Award from Harvard Medical School and a Breast & Gynecologic Cancer Innovation Award from Susan F. Smith Center for Women's Cancers at Dana-Farber Cancer Institute to J.Z. J.A.T. and A.S. are supported by NIH grants P01 CA092548, R35 CA220430, Cancer Prevention Research Institute of Texas (CPRIT) grant RP180813, and a Robert A. Welch Chemistry Chair.

REFERENCES

1. Lord CJ & Ashworth A. PARP inhibitors: Synthetic lethality in the clinic. Science 355, 1152–1158, doi:10.1126/science.aam7344 (2017). [PubMed: 28302823]
2. Farmer H. et al. Targeting the DNA repair defect in BRCA mutant cells as a therapeutic strategy. Nature 434, 917–921, doi:10.1038/nature03445 (2005). [PubMed: 15829967]
3. Bryant HE et al. Specific killing of BRCA2-deficient tumours with inhibitors of poly(ADP-ribose) polymerase. Nature 434, 913–917, doi:10.1038/nature03443 (2005). [PubMed: 15829966]
4. Konstantinopoulos PA, Ceccaldi R, Shapiro GI & D'Andrea AD Homologous Recombination Deficiency: Exploiting the Fundamental Vulnerability of Ovarian Cancer. Cancer Discov 5, 1137–1154, doi:10.1158/2159-8290.CD-15-0714 (2015). [PubMed: 26463832]
5. Ledermann J. et al. Olaparib maintenance therapy in platinum-sensitive relapsed ovarian cancer. N Engl J Med 366, 1382–1392, doi:10.1056/NEJMoa1105535 (2012). [PubMed: 22452356]
6. Coleman RL et al. Rucaparib maintenance treatment for recurrent ovarian carcinoma after response to platinum therapy (ARIEL3): a randomised, double-blind, placebo-controlled, phase 3 trial. Lancet 390, 1949–1961, doi:10.1016/S0140-6736(17)32440-6 (2017). [PubMed: 28916367]

7. Mirza MR et al. Niraparib Maintenance Therapy in Platinum-Sensitive, Recurrent Ovarian Cancer. N Engl J Med 375, 2154–2164, doi:10.1056/NEJMoa1611310 (2016). [PubMed: 27717299]
8. Litton JK et al. Talazoparib in Patients with Advanced Breast Cancer and a Germline BRCA Mutation. N Engl J Med 379, 753–763, doi:10.1056/NEJMoa1802905 (2018). [PubMed: 30110579]
9. Lord CJ & Ashworth A. Mechanisms of resistance to therapies targeting BRCA-mutant cancers. Nat Med 19, 1381–1388, doi:10.1038/nm.3369 (2013). [PubMed: 24202391]
10. Sakai W. et al. Secondary mutations as a mechanism of cisplatin resistance in BRCA2-mutated cancers. Nature 451, 1116–1120, doi:10.1038/nature06633 (2008). [PubMed: 18264087]
11. Ray Chaudhuri A. et al. Replication fork stability confers chemoresistance in BRCA-deficient cells. Nature 535, 382–387, doi:10.1038/nature18325 (2016). [PubMed: 27443740]
12. Noordermeer SM et al. The shieldin complex mediates 53BP1-dependent DNA repair. Nature 560, 117–121, doi:10.1038/s41586-018-0340-7 (2018). [PubMed: 30022168]
13. Ghezraoui H. et al. 53BP1 cooperation with the REV7-shieldin complex underpins DNA structure-specific NHEJ. Nature 560, 122–127, doi:10.1038/s41586-018-0362-1 (2018). [PubMed: 30046110]
14. Ceccaldi R. et al. Homologous-recombination-deficient tumours are dependent on Poltheta-mediated repair. Nature 518, 258–262, doi:10.1038/nature14184 (2015). [PubMed: 25642963]
15. Ceccaldi R, Rondinelli B. & D'Andrea AD Repair Pathway Choices and Consequences at the Double-Strand Break. Trends Cell Biol 26, 52–64, doi:10.1016/j.tcb.2015.07.009 (2016). [PubMed: 26437586]
16. Mateos-Gomez PA et al. Mammalian polymerase theta promotes alternative NHEJ and suppresses recombination. Nature 518, 254–257, doi:10.1038/nature14157 (2015). [PubMed: 25642960]
17. Wood RD & Doublie S. DNA polymerase theta (POLQ), double-strand break repair, and cancer. DNA Repair (Amst) 44, 22–32, doi:10.1016/j.dnarep.2016.05.003 (2016). [PubMed: 27264557]
18. Seki M. et al. High-efficiency bypass of DNA damage by human DNA polymerase Q. EMBO J 23, 4484–4494, doi:10.1038/sj.emboj.7600424 (2004). [PubMed: 15496986]
19. Yoon JH et al. Error-Prone Replication through UV Lesions by DNA Polymerase theta Protects against Skin Cancers. Cell 176, 1295–1309 e1215, doi:10.1016/j.cell.2019.01.023 (2019). [PubMed: 30773314]
20. Chan SH, Yu AM & McVey M. Dual roles for DNA polymerase theta in alternative end-joining repair of double-strand breaks in Drosophila. PLoS Genet 6, e1001005, doi:10.1371/journal.pgen.1001005 (2010). [PubMed: 20617203]
21. Goff JP et al. Lack of DNA polymerase theta (POLQ) radiosensitizes bone marrow stromal cells in vitro and increases reticulocyte micronuclei after total-body irradiation. Radiat Res 172, 165–174, doi:10.1667/RR1598.1 (2009). [PubMed: 19630521]
22. Audebert M, Salles B. & Calsou P. Involvement of poly(ADP-ribose) polymerase-1 and XRCC1/DNA ligase III in an alternative route for DNA double-strand breaks rejoining. J Biol Chem 279, 55117–55126, doi:10.1074/jbc.M404524200 (2004). [PubMed: 15498778]
23. Seki M, Marini F. & Wood RD POLQ (Pol theta), a DNA polymerase and DNA-dependent ATPase in human cells. Nucleic Acids Res 31, 6117–6126 (2003). [PubMed: 14576298]
24. Ozdemir AY, Rusanov T, Kent T, Siddique LA & Pomerantz RT Polymerase theta-helicase efficiently unwinds DNA and RNA-DNA hybrids. J Biol Chem 293, 5259–5269, doi:10.1074/jbc.RA117.000565 (2018). [PubMed: 29444826]
25. Mateos-Gomez PA et al. The helicase domain of Poltheta counteracts RPA to promote alt-NHEJ. Nat Struct Mol Biol 24, 1116–1123, doi:10.1038/nsmb.3494 (2017). [PubMed: 29058711]
26. Zahn KE, Jensen RB, Wood RD & Doublie S. Human DNA polymerase theta harbors DNA end-trimming activity critical for DNA repair. Mol Cell, doi:10.1016/j.molcel.2021.01.021 (2021).
27. Beagan K. et al. Drosophila DNA polymerase theta utilizes both helicase-like and polymerase domains during microhomology-mediated end joining and interstrand crosslink repair. PLoS Genet 13, e1006813, doi:10.1371/journal.pgen.1006813 (2017).
28. Higgins GS & Boulton SJ Beyond PARP-POLtheta as an anticancer target. Science 359, 1217–1218, doi:10.1126/science.aar5149 (2018). [PubMed: 29590065]

29. Yusufzai T. & Kadonaga JT HARP is an ATP-driven annealing helicase. Science 322, 748–750, doi:10.1126/science.1161233 (2008). [PubMed: 18974355]
30. Newman JA, Cooper CDO, Aitkenhead H. & Gileadi O. Structure of the Helicase Domain of DNA Polymerase Theta Reveals a Possible Role in the Microhomology-Mediated End-Joining Pathway. Structure 23, 2319–2330, doi:10.1016/j.str.2015.10.014 (2015). [PubMed: 26636256]
31. Higgins GS et al. A small interfering RNA screen of genes involved in DNA repair identifies tumor-specific radiosensitization by POLQ knockdown. Cancer Res 70, 2984–2993, doi:10.1158/0008-5472.CAN-09-4040 (2010). [PubMed: 20233878]
32. Eder JP, Wheeler CA, Teicher BA & Schnipper LE A phase I clinical trial of novobiocin, a modulator of alkylating agent cytotoxicity. Cancer Res 51, 510–513 (1991). [PubMed: 1985770]
33. Drusano GL et al. Steady-state serum pharmacokinetics of novobiocin and rifampin alone and in combination. Antimicrob Agents Chemother 30, 42–45, doi:10.1128/aac.30.1.42 (1986). [PubMed: 3752982]
34. Kennedy MJ et al. Phase I and pharmacologic study of the alkylating agent modulator novobiocin in combination with high-dose chemotherapy for the treatment of metastatic breast cancer. J Clin Oncol 13, 1136–1143, doi:10.1200/JCO.1995.13.5.1136 (1995). [PubMed: 7738619]
35. Murren JR et al. Phase I and pharmacokinetic study of novobiocin in combination with VP-16 in patients with refractory malignancies. Cancer J 6, 256–265 (2000). [PubMed: 11038146]
36. Liu X. et al. Somatic loss of BRCA1 and p53 in mice induces mammary tumors with features of human BRCA1-mutated basal-like breast cancer. Proceedings of the National Academy of Sciences 104, 12111–12116, doi:10.1073/pnas.0702969104 (2007).
37. Pantelidou C. et al. PARP Inhibitor Efficacy Depends on CD8(+) T-cell Recruitment via Intratumoral STING Pathway Activation in BRCA-Deficient Models of Triple-Negative Breast Cancer. Cancer Discov 9, 722–737, doi:10.1158/2159-8290.CD-18-1218 (2019). [PubMed: 31015319]
38. Turner N, Tutt A. & Ashworth A. Hallmarks of 'BRCAness' in sporadic cancers. Nat Rev Cancer 4, 814–819, doi:10.1038/nrc1457 (2004). [PubMed: 15510162]
39. Taniguchi T. et al. Disruption of the Fanconi anemia-BRCA pathway in cisplatin-sensitive ovarian tumors. Nat Med 9, 568–574, doi:10.1038/nm852 (2003). [PubMed: 12692539]
40. Sugino A, Higgins NP, Brown PO, Peebles CL & Cozzarelli NR Energy coupling in DNA gyrase and the mechanism of action of novobiocin. Proc Natl Acad Sci U S A 75, 4838–4842 (1978). [PubMed: 368801]
41. Marcu MG, Chadli A, Bouhouche I, Catelli M. & Neckers LM The heat shock protein 90 antagonist novobiocin interacts with a previously unrecognized ATP-binding domain in the carboxyl terminus of the chaperone. J Biol Chem 275, 37181–37186, doi:10.1074/jbc.M003701200 (2000). [PubMed: 10945979]
42. Hsieh T. & Brutlag D. ATP-dependent DNA topoisonmerase from D. melanogaster reversibly catenates duplex DNA rings. Cell 21, 115–125, doi:10.1016/0092-8674(80)90119-1 (1980). [PubMed: 6250707]
43. Pocklington MJ, Jenkins JR & Orr E. The effect of novobiocin on yeast topoisomerase type II. Mol Gen Genet 220, 256–260, doi:10.1007/bf00260491 (1990). [PubMed: 2157954]
44. Drean A, Lord CJ & Ashworth A. PARP inhibitor combination therapy. Crit Rev Oncol Hematol 108, 73–85, doi:10.1016/j.critrevonc.2016.10.010 (2016). [PubMed: 27931843]
45. Mirza MR, Pignata S. & Ledermann JA Latest clinical evidence and further development of PARP inhibitors in ovarian cancer. Ann Oncol 29, 1366–1376, doi:10.1093/annonc/mdy174 (2018). [PubMed: 29750420]
46. Parmar K. et al. The CHK1 Inhibitor Prexasertib Exhibits Monotherapy Activity in High-Grade Serous Ovarian Cancer Models and Sensitizes to PARP Inhibition. Clin Cancer Res, doi:10.1158/1078-0432.CCR-19-0448 (2019).
47. Zhou Y, Caron P, Legube G. & Paull TT Quantitation of DNA double-strand break resection intermediates in human cells. Nucleic Acids Research 42, e19–e19, doi:10.1093/nar/gkt1309 (2013). [PubMed: 24362840]
48. Feng W. et al. Genetic determinants of cellular addiction to DNA polymerase theta. Nat Commun 10, 4286, doi:10.1038/s41467-019-12234-1 (2019). [PubMed: 31537809]

49. Johnson N. et al. Stabilization of mutant BRCA1 protein confers PARP inhibitor and platinum resistance. Proc Natl Acad Sci U S A 110, 17041–17046, doi:10.1073/pnas.1305170110 (2013). [PubMed: 24085845]

50. Yazinski SA et al. ATR inhibition disrupts rewired homologous recombination and fork protection pathways in PARP inhibitor-resistant BRCA-deficient cancer cells. Genes Dev 31, 318–332, doi:10.1101/gad.290957.116 (2017). [PubMed: 28242626]

51. Lemee F. et al. DNA polymerase theta up-regulation is associated with poor survival in breast cancer, perturbs DNA replication, and promotes genetic instability. Proc Natl Acad Sci U S A 107, 13390–13395, doi:10.1073/pnas.0910759107 (2010). [PubMed: 20624954]

52. Barber LJ et al. Comprehensive genomic analysis of a BRCA2 deficient human pancreatic cancer. PLoS One 6, e21639, doi:10.1371/journal.pone.0021639 (2011).

53. Eckelmann BJ et al. XRCC1 promotes replication restart, nascent fork degradation and mutagenic DNA repair in BRCA2-deficient cells. NAR Cancer 2, zcaa013, doi:10.1093/narcan/zcaa013 (2020).

Methods-only References

54. Zhou J. et al. Human CHD1 is required for early DNA-damage signaling and is uniquely regulated by its N terminus. Nucleic Acids Res 46, 3891–3905, doi:10.1093/nar/gky128 (2018). [PubMed: 29529298]

55. Staudenbauer WL & Orr E. DNA gyrase: affinity chromatography on novobiocin-Sepharose and catalytic properties. Nucleic Acids Res 9, 3589–3603, doi:10.1093/nar/9.15.3589 (1981). [PubMed: 6269086]

56. Lim KS et al. USP1 Is Required for Replication Fork Protection in BRCA1-Deficient Tumors. Mol Cell 72, 925–941 e924, doi:10.1016/j.molcel.2018.10.045 (2018).

57. Liu JF et al. Establishment of Patient-Derived Tumor Xenograft Models of Epithelial Ovarian Cancer for Preclinical Evaluation of Novel Therapeutics. Clin Cancer Res 23, 1263–1273, doi:10.1158/1078-0432.CCR-16-1237 (2017). [PubMed: 27573169]

58. Harder E. et al. OPLS3: A Force Field Providing Broad Coverage of Drug-like Small Molecules and Proteins. J Chem Theory Comput 12, 281–296, doi:10.1021/acs.jctc.5b00864 (2016). [PubMed: 26584231]

59. Friesner RA et al. Extra precision glide: docking and scoring incorporating a model of hydrophobic enclosure for protein-ligand complexes. J Med Chem 49, 6177–6196, doi:10.1021/jm051256o (2006). [PubMed: 17034125]

60. Knight JL et al. Leveraging Data Fusion Strategies in Multireceptor Lead Optimization MM/GBSA End-Point Methods. J Chem Theory Comput 10, 3207–3220, doi:10.1021/ct500189s (2014). [PubMed: 26588291]

SIGNIFICANCE:

We identified Novobiocin as a specific POLθ inhibitor that selectively kills naïve and PARPi resistance HR-deficient tumors *in vitro* and *in vivo.* This first-in-class POLθ inhibitor can potentially be a novel therapy for HR-deficient tumors as monotherapy or in combination with PARPi.

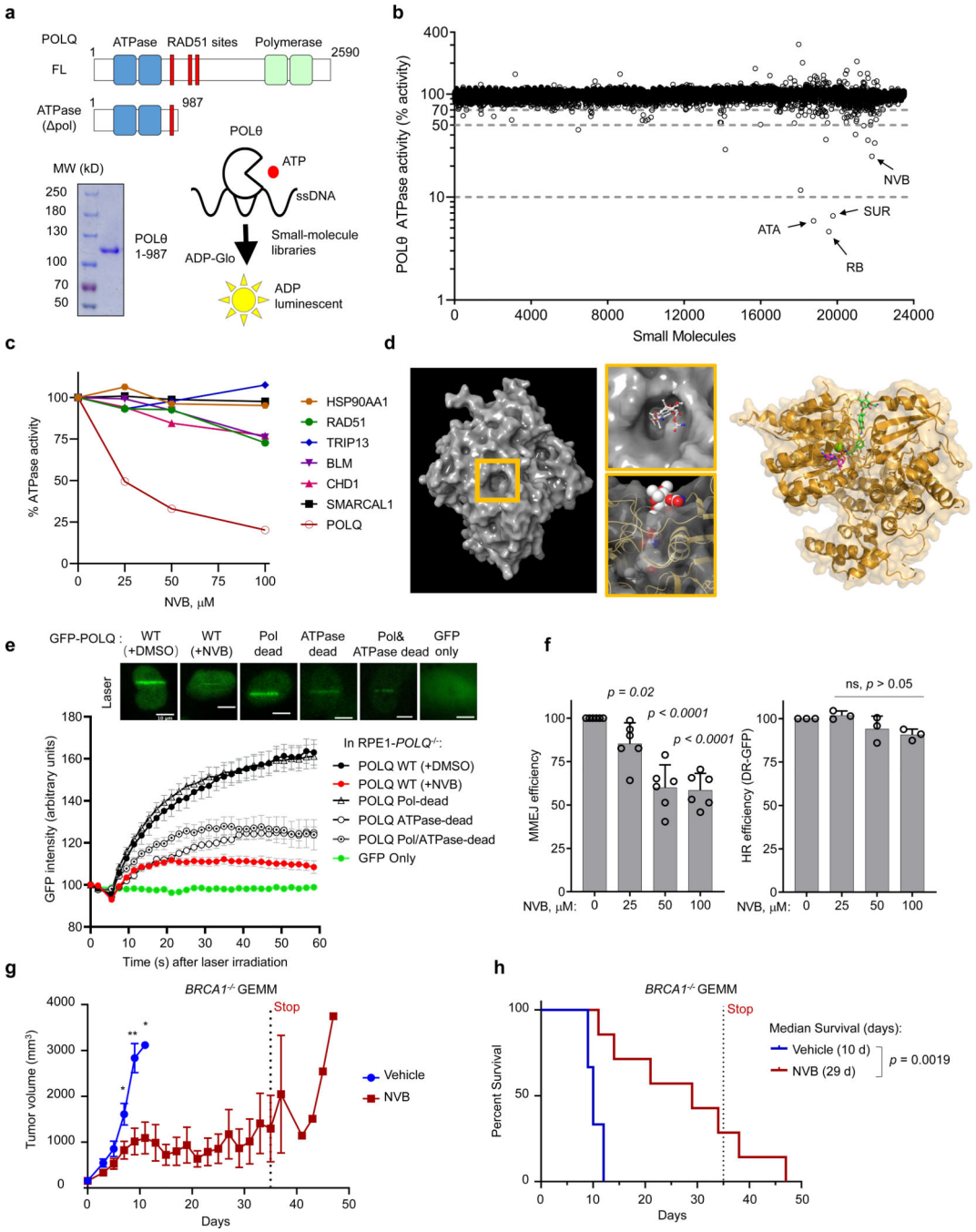

Fig. 1. A small-molecule screen identifies Novobiocin (NVB) as a specific POLθ ATPase inhibitor that kills HR-deficient tumors.

a, The domain structures of full length (FL) and ATPase domain (ΔPol, a.a. 1–987) of POLθ, a Coomassie-stained gel of the purified POLθ ATPase domain used for screen, and a schematic of the small molecule screen. **b**, Results of the small-molecule screen. Shown is POLθ ATPase activity in the presence of small-molecule libraries (enriched with bioactive compounds). Four top hits verified in the secondary screen (Extended Data Fig. 1b) were labeled: reactive blue 2 (RB), suramin (SUR), novobiocin (NVB) and aurintricarboxylic acid

(ATA). Data are mean from n = 2 replicates. **c**, Quantification of the ATPase activity of POLθ, SMARCAL1, CHD1, BLM, TRIP13, RAD51 and HSP90AA1 with increasing concentration of NVB. ATPase activity was determined by ADP-Glo assay (Promega). Activities were normalized to DMSO (0.1%). Mean of 6 replicates from n = 2 two independent experiments are shown. **d**, The NVB binding tunnel in POLθ ATPase domain (shown in surface - PDB 5AGA) was predicted by extra precision glide docking and lowest binding free energy from prime MM-GBSA calculations to have multiple hydrogen bonds and close hydrophobic packing. Top and side views showing NVB docking into the tunnel. Binding modes of NVB (green sticks) and AMP-PNP (magenta sticks) in POLθ helicase domain (PDB 5AGA) with green sphere showing active site Mg^{2+} ion. **e**, Quantification and representative images of POLθ-GFP accumulation at sites of laser micro-irradiated DNA damage in RPE1-*POLQ*$^{-/-}$ cells overexpressing GFP-tagged POLQ WT, polymerase mutant, ATPase/Helicase mutant, or double mutant. GFP-POLQ WT expressing cells treated with DMSO (0.1%) or 100 μM of NVB were shown. Mean ± SEM were shown. WT(+DMSO), n = 7 cells; WT(+NVB), n = 8 cells; Pol dead, n = 24 cells; ATPase dead, n = 13 cells; Pol/ATPase dead, n= 14 cells, from three independent experiments. GFP only, n = 4, from two independent experiments. **f**, MMEJ and HR repair reporter assays in U2OS cells treated with increasing concentration of NVB. Percentage of GFP positive cells are shown as pathway efficiency. Mean ± SD, from n = 6 (for MMEJ) and n = 3 (for HR) from three independent experiments, ordinary one-way ANOVA. **g**, Tumor growth of the GEMM model (*Brca1*$^{-/-}$ TNBC) after treatment with vehicle (PBS) or NVB. Tumor bearing FVB/129P2 were treated with PBS or 100 mg/kg NVB via IP injection twice a day for 5 weeks. Mean ± SEM is shown, n = 6 mice for PBS group and n = 7 mice for NVB group. **h**, Survival plot of the experiment shown in (**g**). Median survival and *p* value are shown, Statistical analyses in **g** and **h** were two-tailed *t*-test. *, $p < 0.05$. **, $p < 0.01$.

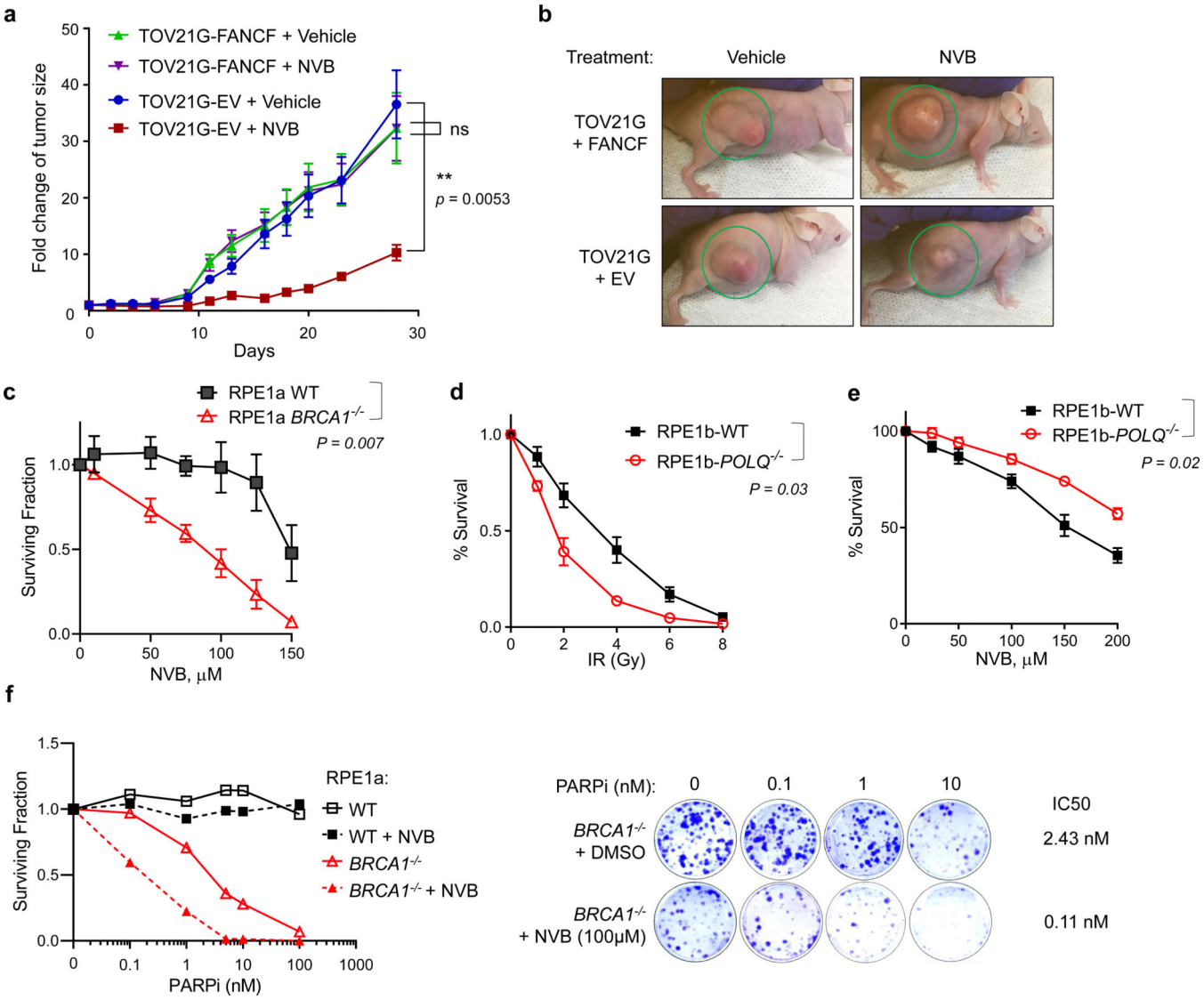

Fig. 2. NVB kills HR-deficient tumors *in vivo* and *in vitro* and synergizes with PARPi.

a, Tumor growth of the xenograft model with TOV21G (FANCF deficient ovarian cancer) or FANCF-complemented TOV21G cells. The tumor bearing mice were treated with vehicle or 100 mg/kg NVB via IP injection twice a day for 4 weeks. Fold change of tumor was calculated using the formula Fold = T/T0, where T is the tumor size at given time and T0 is the initial tumor size. Data are Mean ± SEM, from n = 10 mice in each group. Statistical analysis was Dunn's multiple comparisons test. **b**, Representative images of TOV21G xenograft tumors at the end of NVB treatment. **c,** Clonogenic survival of *BRCA1*$^{-/-}$ and WT RPE1 cells under increasing concentrations of the POLθ inhibitor NVB. Survival is normalized to the untreated sample. Data shown are mean ± SEM, n = 3 independent experiments. **d**, IR sensitivity of WT and *POLQ*$^{-/-}$ RPE1 cells in clonogenic assays. **e**, NVB sensitivity of WT and *POLQ*$^{-/-}$ RPE1 cells. Data shown in **d** and **e** are mean ± SD, from n = 6 biological replicates. Significance in **c-e** were determined by paired t-test, two-tailed. **f,** Clonogenic survival of *BRCA1*$^{-/-}$ and WT RPE1 cells under increasing concentrations of

the PARPi (Rucaparib) alone or in combination with NVB. Quantifications of survival fraction (mean from n=2 independent experiments), representative images and calculated IC50 values are shown.

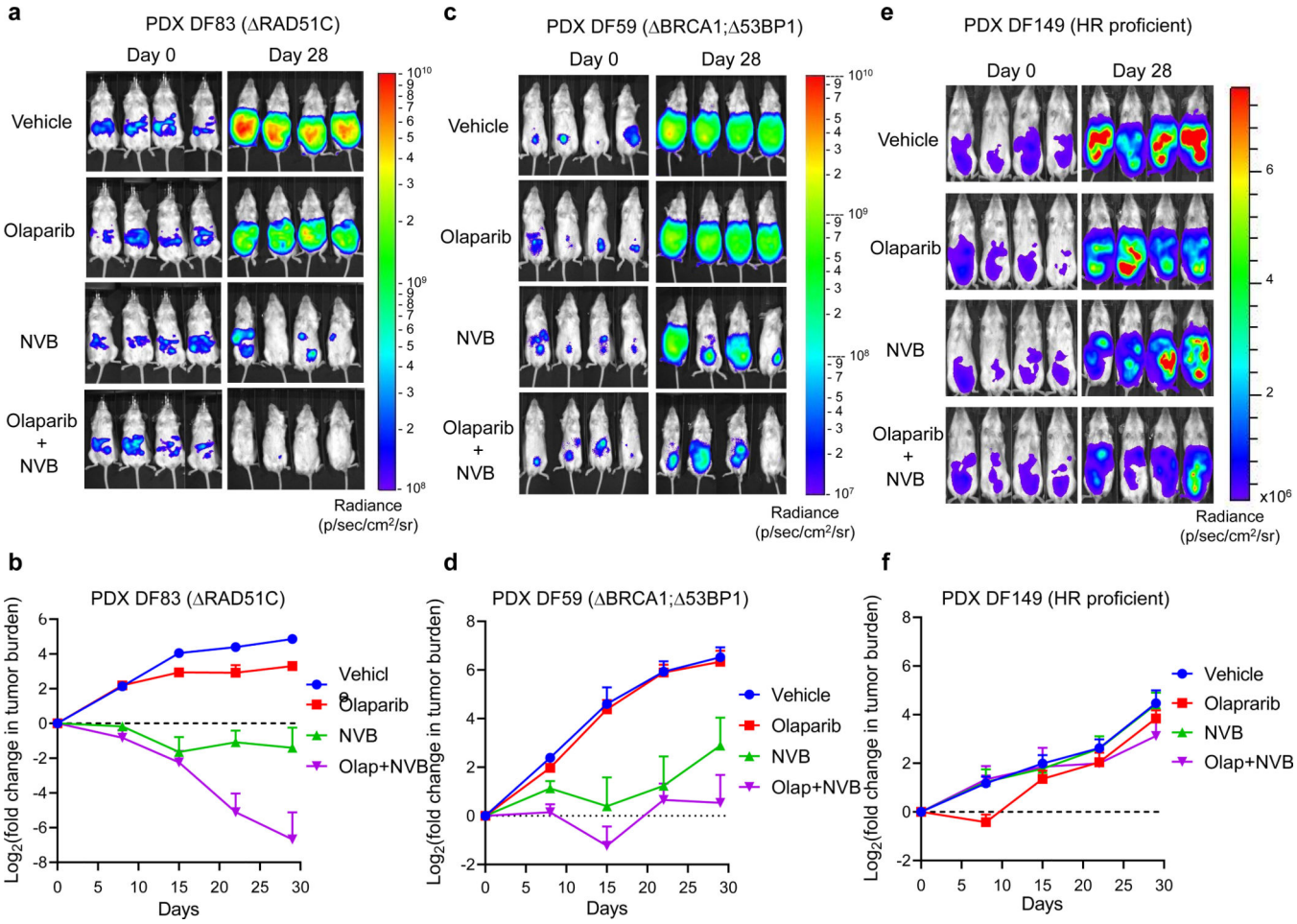

Fig. 3. NVB kills HR-deficient tumors and overrides PARPi resistance *in vivo* in PDX models.

a-b, Efficacy of NVB in PDX model DF83 (RAD51C deficient). NSG mice (n = 7 mice/group) bearing luciferized DF83 cells derived from an ovarian cancer patient were treated with 50 mg/kg of olaparib (daily, orally), 75 mg/kg NVB (via IP, b.i.d.), or both for 4 weeks. Tumor growth was monitored weekly by bioluminescence imaging. Representative images of tumor burden on day 0 and day 28 are shown, and quantifications shown are mean ± SEM, n = 8 mice. Log_2(fold change in tumor size) was calculated using the formula log_2(T/T0), where T is the tumor volume at given time and T0 is the initial tumor volume. **c-d**, Efficacy of NVB in PARPi resistant PDX model DF59 (BRCA1-deficient, 53BP1 loss), n = 6 mice/group. Same conditions and analysis were applied as in **a-b**. **e-f**, Efficacy of NVB in PARPi resistant PDX model DF149 (BRCA1-WT, HR proficient), n = 7 mice/group. Same conditions and analysis were applied as in **a-b**.

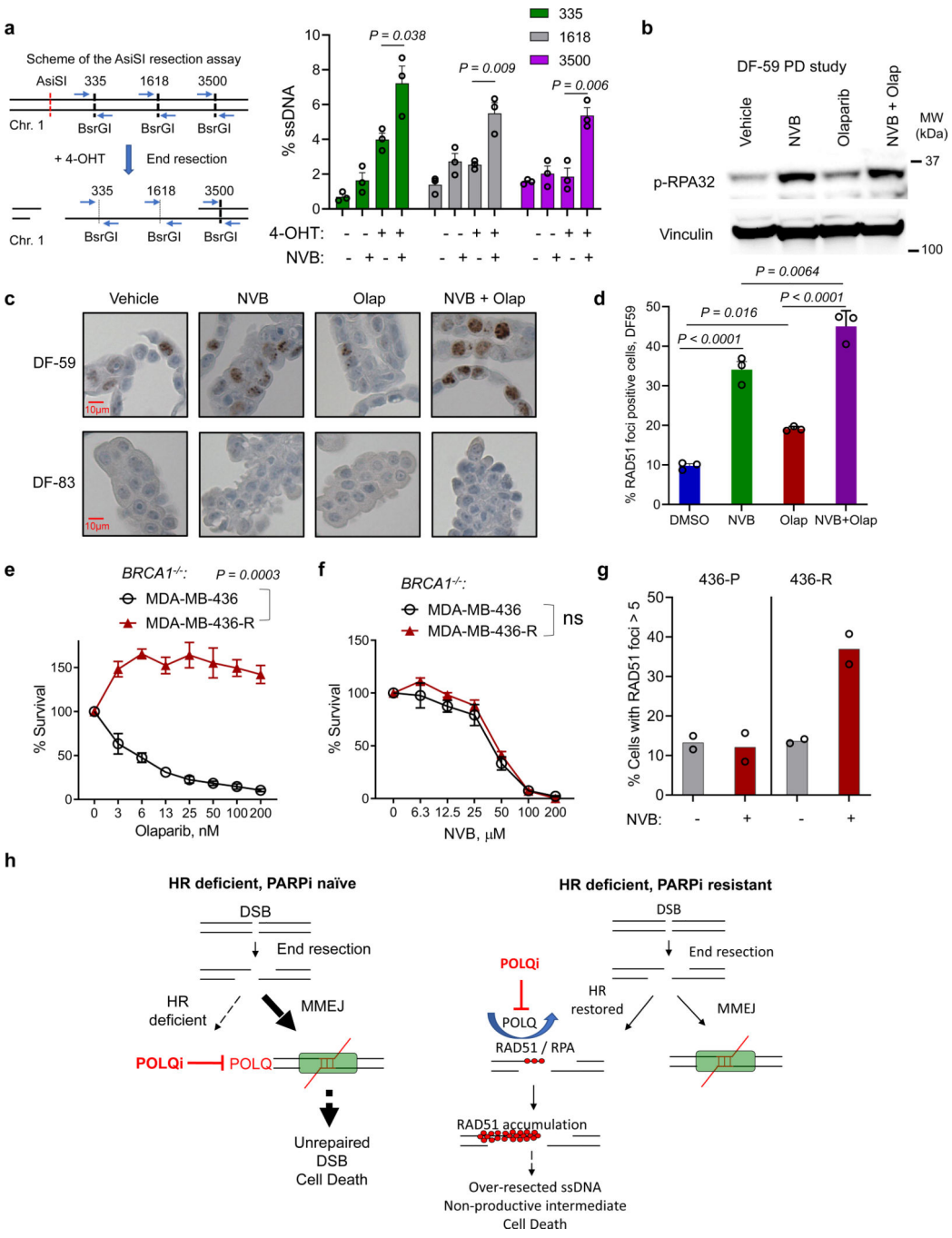

Fig. 4. NVB induces excessive DSB end resection and non-productive RAD51 foci.

a, DSB end resection assay in U2OS cells with or without NVB. A scheme of the AsiSI resection assay is shown. Cells were incubated with 100 μM NVB for 18 h and then 4-OHT for 4 h. Genomic DNA were isolated to analyze %ssDNA flanking the AsiSI DSB site at indicated positions, using BrsGI digestion and qPCR quantification. Mean ± SEM, n = 3 independent experiments, two tailed unpaired *t-test*. **b**, Western blot analysis of phosphor-RPA32 in PD samples of the DF59 PDX model, 52 hours after first dose. Tumor bearing mice were dosed as in efficacy study in Fig. 3. **c-d**, Representative IHC images and

quantifications of RAD51 foci in DF-59 and DF-83 PDX models. FFPE sections of the isolated tumor cells (as described in **b**) were stained with a RAD51 antibody. %RAD51-foci positive cells (> 4 foci/cell) in 3 random 40X fields was estimated in DF-59. No RAD51 focus was observed in the DF-83 model. Data shown are Mean±SD, n=3 tumors, ordinary one-way ANOVA Bonferroni's multiple comparisons test. **e-f**, CellTiter-Glo cell viability assay in parental MDA-MB-436 (*BRCA1*-mutated) and PARPi-resistant MDA-MB-436-R cells under increasing concentration of Olaparib **(e)** or NVB **(f)**. Mean ± SEM are shown, with n = 6 independent cultures. ns, no significant, two-tailed paired *t*-test. **g**, RAD51 foci assay with DMSO or NVB in MDA-MB-436 or MDA-MB-436-R. Cells with more than 5 foci were counted as positive. Data were mean from two independent experiments. **h**, A scheme shows the mechanism of NVB cytotoxicity in PARPi naïve and resistant tumor cells. In PARPi naïve HR-deficient settings, cells rely on MMEJ to repair DSBs. NVB inhibits MMEJ repair and causes unrepaired DSBs, leading to cell death. In HR-deficient but PARPi resistant settings, NVB inhibits the counteracting function of POLθ on RPA and RAD51, leading to enhanced DSB resection, accumulation of non-functional RAD51 foci, unrepaired DSBs and eventually cell death.

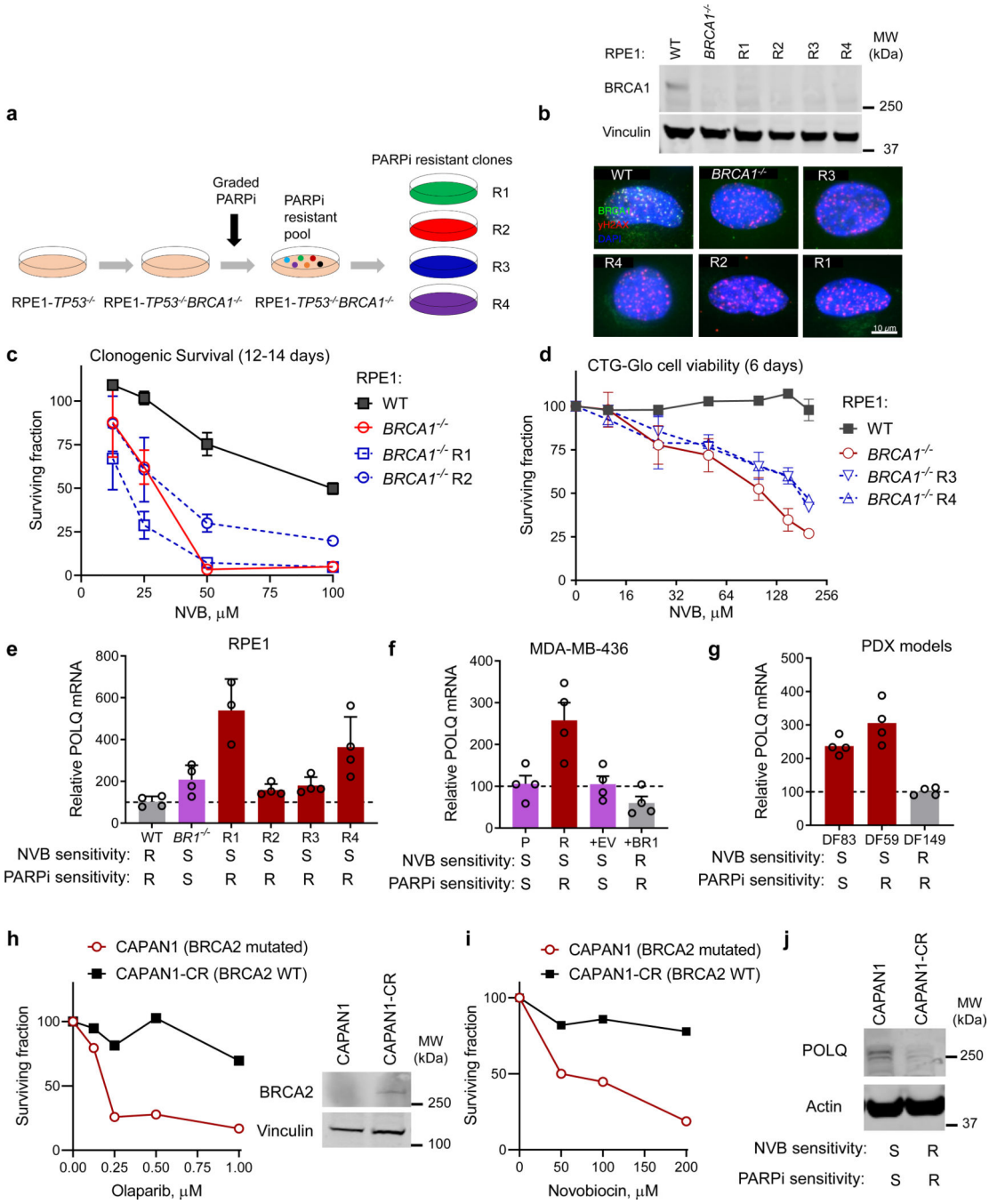

Fig. 5. NVB overcomes multiple PARPi resistance mechanisms and POLQ expression level is a predictive biomarker for NVB sensitivity.

a. A schematic shows how the PARPi resistant clones R1-R4 were generated. **b**. A Western blot of WT and *BRCA1*$^{-/-}$ RPE1 cells and the PARPi resistant clones, using an anti-BRCA1 antibody (Millipore #OP92). No BRCA1 reversion was observed in the clones. **c-d.** NVB sensitivity of WT RPE1, *BRCA1*$^{-/-}$ RPE1, and PARPi-resistant *BRCA1*$^{-/-}$ clones (R1-R4). R1 was selected by olaparib and R2-R4 were selected by Niraparib. R1 and R2 were tested in clonogenic survival assays (12–14 days) **(c)**. R3 and R4 were tested in CellTiter-Glo cell

viability assay (6 days) (**d**). Data are mean ± SEM, n = 3 independent cultures. **e**. POLQ expression at mRNA level and protein level in WT RPE1, *BRCA1*$^{-/-}$ RPE1, and PARPi-resistant *BRCA1*$^{-/-}$ clones (R1-R4). POLQ mRNA was measured by qRT-PCR and normalized to beta-Actin (ACTB). Mean ± SD of n=4 independent cultures. **f**. POLQ expression at mRNA level in parental (P), PARPi resistant (R), and empty vector (+EV) or BRCA1-cDNA (+BR1) complemented MDA-MB-436 cells. Mean ± SD of n=4 independent cultures. **g**. POLQ expression at mRNA level in PDX models DF53, DF83 and DF149. Mean of 4 technical replicates for each PDX model are shown. **h**. Olaparib sensitivity of CAPAN1 (BRCA2 mutated) and CAPAN1-CR cells (BRCA2 CRISPR edited back to wild type) in clonogenic survival assays. **i**. NVB sensitivity of CAPAN1 and CAPAN1-CR cells in clonogenic survival assays. Mean of n=2 independent experiments are shown in **h** and **i**. Statistical analysis in **h** and **i** were paired t-test, *$p < 0.05$, **j**. The expression levels of POLQ in CAPAN1 and CAPAN1-CR cells, analyzed by Western blotting.